REPORT DOCUMENTATION PAGE

Form Approved OMB NO. 0704-0188

Public Reporting Burden for this collection of information is estimated to average 1 hour per response, including the time for reviewing instructions, searching existing data sources, gathering and maintaining the data needed, and completing and reviewing the collection of information. Send comment regarding this burden estimate or any other aspect of this collection of information, including suggesstions for reducing this burden, to Washington Headquarters Services, Directorate for Information Operations and Reports, 1215 Jefferson Davis Highway, Suite 1204, Arlington VA, 22202-4302, and to the Office of Management and Budget, Paperwork Reduction Project (0704-0188), Washington DC 20503

1. AGENCY USE ONLY (Leave Blank)	2. REPORT DATE:	3. REPORT TYPE AND DATES COVERED
		Final Report 1-Apr-2005 - 31-Dec-2005

4. TITLE AND SUBTITLE
Reliable Prescreening of Candidate NerveAgent Prophylaxes via 3D QSAR

5. FUNDING NUMBERS
W911NF0510181

6. AUTHORS
Gerald H. Lushington, Jian-Xin Guo, Nora M. Wallace

8. PERFORMING ORGANIZATION REPORT NUMBER

7. PERFORMING ORGANIZATION NAMES AND ADDRESSES
University of Kansas
2385 Irving Hill Road

Lawrence, KS   66044 -7552

9. SPONSORING/MONITORING AGENCY NAME(S) AND ADDRESS(ES)

U.S. Army Research Office
P.O. Box 12211
Research Triangle Park, NC 27709-2211

10. SPONSORING / MONITORING AGENCY REPORT NUMBER

46918-CH-II.1

11. SUPPLEMENTARY NOTES
The views, opinions and/or findings contained in this report are those of the author(s) and should not contrued as an official Department of the Army position, policy or decision, unless so designated by other documentation.

12. DISTRIBUTION AVAILIBILITY STATEMENT
Approved for Public Release; Distribution Unlimited

12b. DISTRIBUTION CODE

13. ABSTRACT (Maximum 200 words)
The abstract is below since many authors do not follow the 200 word limit

The abstract is below since many authors do not follow the 200 word limit

14. SUBJECT TERMS
nerve agents, acetylcholinesterase, prophylaxis, QSAR, virtual screening, noncovalent inhibitors

15. NUMBER OF PAGES
Unknown due to possible attachments

16. PRICE CODE

17. SECURITY CLASSIFICATION OF REPORT	18. SECURITY CLASSIFICATION ON THIS PAGE	19. SECURITY CLASSIFICATION OF ABSTRACT	20. LIMITATION OF ABSTRACT
UNCLASSIFIED	UNCLASSIFIED	UNCLASSIFIED	UL

NSN 7540-01-280-5500

Standard Form 298 (Rev .2-89)
Prescribed by ANSI Std.
239-18 298-102

Report Title

Final Report: Reliable Prescreening of Candidate NerveAgent Prophylaxes via 3D QSAR

ABSTRACT

Organophosphorus (OP) nerve agents are among the most toxic chemicals known to man and are notoriously easy to synthesize. As a result, their potential use against our military by insurgents, terrorists and other rogue groups remains a continuing threat. Therapeutics for countering OP toxicity exist, but do not adequately protect against some fast-acting agents (e.g., soman) without complementary support of prophylactic species. Some prophylactics do already exist, but may be responsible for unacceptable long-term health consequences. As a result, the search for safe, effective OP prophylactics remains of great interest. OP prophylactic design typically involves finding inhibitors of the acetylcholinesterase (AChE) active site (the target of OP toxicity) that bind strongly enough to prevent OP binding, but not so strongly as to be excessively toxic themselves. Searching such a balance through laboratory experiments alone is likely to entail an expensive, inefficient trial-and-error search. In order to expedite such efforts we have developed and applied computational quantitative structure-activity relationship models to the prediction of AChE-binding efficacy and toxicity for candidate prophylactics, identifying six strong inhibitor prospects (predicted to have sub-nanomolar Ki-values) from within the synthetically available chemicals of the NIH PubChem database.

List of papers submitted or published that acknowledge ARO support during this reporting period. List the papers, including journal references, in the following categories:

(a) Papers published in peer-reviewed journals (N/A for none)

Guo, J., Hurley, M.M., Wright, J.B., Lushington, G.H. "A Docking Score Function for Estimating Ligand-Protein Interactions: Applications to Acetylcholinesterase Inhibition." J. Med. Chem. 47: 5492, 2004.

Hurley, M.M., Balboa, A., Lushington, G.H., and Guo, J.-X. "Interactions of Organophosphorus and Related Compounds with Cholinesterases, a Theoretical Study." Chemico-Biological Interactions. 157-158: 321-325, 2005.

Lushington, G.H., Guo, J.-X., Hurley, M.M. "Acetylcholinesterase: Molecular Modeling with the Whole Toolkit." Curr. Topics Med. Chem. 6: 57-73, 2006.

Guo, J.-X., Wu, J.-Q., Wright, J.B., Lushington, G.H. "Mechanistic Insight into Acetylcholinesterase Inhibition and Acute Toxicity of Organophosphorus Compounds: a Molecular Modeling Study." Chem. Res. Toxicol. 19: 209-216, 2006.

Number of Papers published in peer-reviewed journals: 4.00

(b) Papers published in non-peer-reviewed journals or in conference proceedings (N/A for none)

Number of Papers published in non peer-reviewed journals: 0.00

(c) Papers presented at meetings, but not published in conference proceedings (N/A for none)

Guo, J.-X.; Lushington, G.H.; The Mechanistic Insight by Molecular Modeling on The Acute Toxicity of Organophosphorus Compounds. Kansas city area life sciences research day, April 6, 2005

Number of Papers not Published: 1.00

(d) Manuscripts

Number of Manuscripts: 0.00

Number of Inventions:

Graduate Students

NAME	PERCENT_SUPPORTED
FTE Equivalent:	
Total Number:	

Names of Post Doctorates

NAME	PERCENT_SUPPORTED
FTE Equivalent:	
Total Number:	

Names of Faculty Supported

NAME	PERCENT_SUPPORTED
FTE Equivalent:	
Total Number:	

Names of Under Graduate students supported

NAME	PERCENT_SUPPORTED
FTE Equivalent:	
Total Number:	

Names of Personnel receiving masters degrees

NAME
Total Number:

Names of personnel receiving PHDs

NAME
Total Number:

Names of other research staff

NAME	PERCENT_SUPPORTED	
Jian-Xin Guo	0.75	No
Nora M. Wallace	0.00	No
FTE Equivalent:	**0.75**	
Total Number:	**2**	

Sub Contractors (DD882)

Reliable Prescreening of Candidate Nerve Agent Prophylaxes via 3D QSAR

Final Report
Gerald H. Lushington, Nora M. Wallace and Jian-Xin Guo
The University of Kansas

Forward: This work was aimed at developing and implementing a reliable, efficient computational method for predicting the propensity of specific chemicals to serve as prophylaxes against nerve agent poisoning. Based on three dimensional (3D) quantitative structure-activity relationship (QSAR) criteria, the method was designed to identify those Acetylcholinesterase (AChE) inhibitors that either bind too weakly (i.e., are ineffectual) or too strongly (i.e., are themselves toxic) from the myriad of known AChE inhibitors. The resulting tool should thus expedite DOD prophylaxis research by screening out compounds with inappropriate inhibition tendencies.

This project aims to deliver software capable of deriving quantitatively reasonable binding affinity predictions from docked ligand-receptor complexes, thus allowing estimation of potential appliation to nerve agent prophylaxis. Conventional docking scoring functions whose entropic term has been trained across a broad range of enzyme receptors seem to score AChE interactions very poorly. To properly account for AChE entropy, we will use QSAR techniques to train an AChE-specialized scoring model as a weighted linear sum of ligand atom - receptor residue enthalpic interactions. The predictions generated by this software need not replace more rigorous experimental or computational measurements, but should permit prescreening that will help researchers to focus their efforts on manageable subsets of the extensive collection of known or suspected AChE inhibitors. This work is also expected to provide an efficient means for intuiting new inhibitor scaffolds by elucidating the steric and electrostatic importance of specific receptor residues whose interactions must be accomodated by bound ligands.

Tables and Figures:
- Figure 1. Schematic showing the information flow into and within our AChE ligand binding affinity prediction (scoring) software.
- Table 1. Predicted AChE binding affinity for 71 molecules from the PubChem Small Molecules Collection with physicochemical attributes similar to known AChE inhibitors.
- Figure 2. Top scoring AChE inhibitors from derived from PubChem analogs of known anticholinesterases
- Figure 3. Bound conformations of molecules 1144141 (A), and 101917 (B) within the AChE active site.

Problem Statement: identification of strong but non-toxic AChE inhibitors is critical to continued efforts to devise a safe and reliable prophylaxis scheme for countering the toxic potential of nerve agent chemical weaponry. *In vitro* and *in vivo* pursuit of such research is inherently dangerous, time consuming and expensive, thus the development of reliable new computational methods to prescreen potential inhibitor candidates is of great potential value. Given multiple crystal structures of AChE available in the literature and within the protein databank, this research is highly amenable to structure-based design techniques, however the inhibition scoring models provided with conventional molecular docking software do not correlate well with experimental affinity trends among known AChE inhibitors, Likely due to an inaccurate or inadequate account of entropic effects within the AChE receptor. We have thus a scoring model in this work to reliably

account for such effects and thereby reproduce known behavior and predict efficacy of hitherto uncharacterized compounds.

Important Results: The basic methodology underlying this work was developed, validated and published [1] prior to commencement of this project. The corresponding publication is provided as Appendix A.   The primary deliverable in this project, the development of software implementing the resulting AChE-inhibition specific score function for use by chemical defense researchers (described below) was completed by 9/30/2005. Use of the resulting software entails a process flow as depicted in Figure 1, whereby a researcher applies our specially tailored AChE-specific score function to evaluate the inhibitive potential for ligands that have been computationally or manually docked to the AChE receptor.   The actual computational docking simulation is a prerequisite to our analysis and is not explicitly performed via the software developed herein, although our method is compatible with the docking results attained by most available docking programs, including commercial codes such as FlexX and MOE-Dock, plus academic freeware codes such as AutoDock. An additional co-requisite step, the assignment of Merck Molecular Force Field (MMFF94) atom types and partial charges [2] must also be performed independently of our software, as can be readily accomplished by a variety of 3rd party programs such as QUACPAC, SYBYL, MOE, etc. Given the docked structure and the proper MMFF94 atom types, one may then apply our new programs compute a pK_i score for the ligand via the expression described in detail

Fig. 1. Schematic showing the information flow into and within our AChE ligand binding affinity prediction (scoring) software.
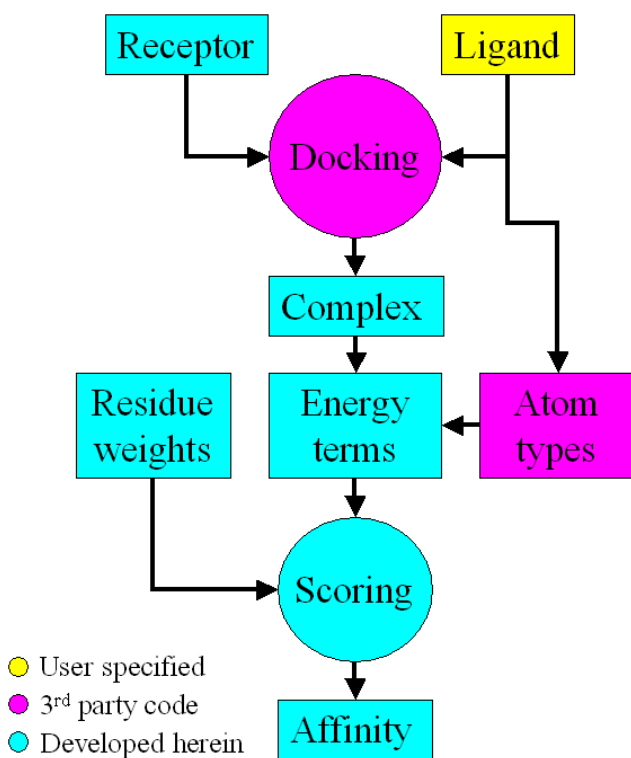
Compatible Software

Ligand model preparation:
Chem3D (commercial)
  http://www.cambridgesoft.com
ChemSketch (free for non-profit)
  http://www.acdlabs.com
Insight-II (commercial)
  http://www.accelrys.com
MOE (commercial)
  http://www.chemcomp.com
MOLDA (free for non-profit)
  http://www.molda.org
SYBYL (commercial)
  http://www.tripos.com

Docking:
AutoDock (free for non-profit)
  http://www.scripps.edu/mb/olson
FlexX (commercial)
  http://www.tripos.com
MOE-Dock (commercial)
   http://www.chemcomp.com

Atom typing / charge calculation:
QUACPAC (free for non-profit)
  http://www.eyesopen.com
SYBYL (commercial)
http://www.tripos.com

in Eq. 1 of Appendix A. Specifically, ligand / receptor residue electrostatic and van der Waals intermolecular interaction enthalpy terms are computed according to the MMFF94 force field terms as devised by Thomas Halgren [1]. These enthalpies are translated to final predicted pK_i affinity predictions by incorporating entropic perturbative corrections (for each receptor residue within a 12 Å sphere of the central cavity) as evaluated by partial least squares (PLS) fitting to affinity trends within a set of 53 known non-covalent AChE inhibitors. In carrying out this PLS modeling, we achieved an excellent correlation ($R^2 = 0.89$) relative to experimental affinity data, as well as strong predictivity (leave-one-out cross validated correlation of $Q^2 = 0.71$ within the training set and a predictive $R^2 = 0.69$ value for a set of 16 compounds left out of the original training set).

Work during the final three months of CY2005 was devoted to the application of our method to elucidation of new potential inhibitors. To accomplish this, then entire PubChem small molecule virtual library (millions of compounds) was scanned via the DiverseSolutions[TM] [3] program to elucidate recently synthesized compounds with physicochemical properties similar (but not identical) to those known AChE inhibitors in the original 69 compound training and test sets reported in the previous paragraph. From this analysis, a total of 71 potential new inhibitor candidates were elucidated according to minimal physicochemical distances as scored by BCUT diversity metrics [4]. This set of compounds were then docked into an AChE receptor model via the FlexX program [5], and computational pK_i predictions were then performed. The resulting affinity scores are reported in Table 1, and the five top scoring (sub-nanomolar) inhibitors are depicted in Fig. 2.

Table 1. Predicted AChE binding affinity for 71 molecules from the PubChem Small Molecules Collection with physicochemical attributes similar to known AChE inhibitors. potential sub-nanomolar inhibitors (pKi > 9.0) are shown in bold font.

Cpd. ID	pK_i	Cpd. ID	pK_i	Cpd. ID	pK_i	Cpd. ID	pK_i
3389	6.4707	680250	8.6312	933051	5.7801	1339872	7.3119
138357	7.4426	720003	5.6345	951510	6.9074	1341521	7.6272
184705	8.9626	**748308**	**10.1534**	956831	5.5098	1379265	7.2713
191042	7.6288	748321	5.7561	956837	6.4678	1410811	5.4950
210342	8.7880	775240	3.3730	986516	4.5478	1427301	8.1817
249033	**10.8281**	783427	7.0665	**1001917**	**10.6315**	1430079	5.7702
266808	4.3691	783500	7.7037	1133586	7.9118	1464709	6.9736
270535	5.3963	785217	7.4220	**1144141**	**14.2625**	1467950	-8.0860
281236	7.0434	798534	7.4776	1150763	7.5349	1563954	6.7446
376530	8.6967	802115	7.8668	1152275	7.2546	1586860	5.9723
376534	8.8889	802520	1.2580	1152327	7.2546	1629088	8.4024
409286	8.1989	833602	6.2348	1154309	6.0770	1637355	6.6228
427257	3.5223	838412	7.7260	1163388	6.1331	1637358	7.3683
434434	6.2186	848206	7.1518	1167962	6.7236	1637361	7.2771
493838	6.9859	858800	8.9556	1179804	6.5368	**1639895**	**9.0748**
495057	6.9699	881012	6.8794	1236539	6.8997	1658324	7.2574
498062	7.4259	899731	8.7880	1316823	7.0958	1665392	8.4541
625525	8.7682	919226	7.5994	1333763	6.2979		

Among the top scoring prophylactic candidates that we identified, the one predicted to be the most powerful inhibitor, molecule #1144141, is a tacrine-line peripheral-active-site (PAS) binder whose docked conformation is reported in Fig. 3a. Molecules 249033 and 748308, and 1639895 have similar PAS-binding conformations. Molecule #101917, on the other hand, binds one tail in the PAS region and another down near the base of the AChE gorge in a manner, shown in Fig. 3b, that is analogous to the well known Alzheimer's disease drug aricept (donepezil).
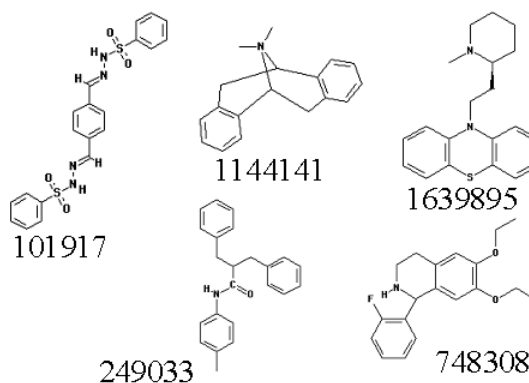
Fig.2. Top scoring AChE inhibitors from derived from PubChem analogs of known anticholinesterases.
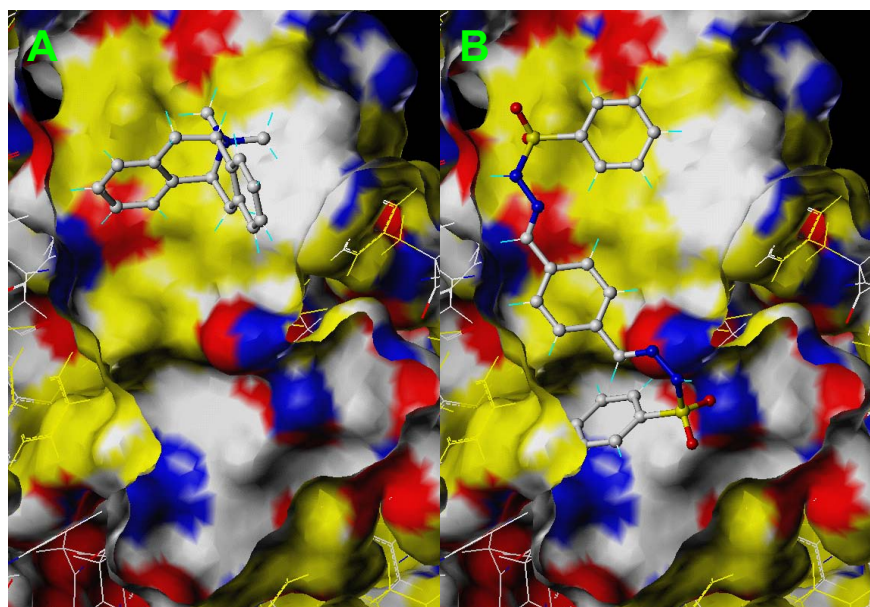
Fig. 3. Bound conformations of molecules 1144141 (A), and 101917 (B) within the AChE active site. The receptor surface is colored as follows: red = H-bond acceptors (O's and lone pair N's), blue = donatable H's (HO and HN), white = other polar atoms, yellow = nonpolar atoms. Ligands are colored according to standard CPK coloring (H = cyan, C = white, N = blue, O = red, S = yellow).

Although molecule #1144141 is clearly predicted to be the stronger inhibitor, it has two potential drawbacks: a) while it's predicted affinity may be a significant over-estimation (since there were no inhibitors in the training set within orders of magnitude of the same affinity) it may still be too powerful an inhibitor and may thus effect an intolerable level of AChE-inhibition-related toxicity, and b) deriving most of its inhibitive potential from PAS hydrophobic interactions, like tacrine, may significantly diminish the oral availability and distributive potential of the molecule. Consequently, molecule #101917 and its analogs, essentially exhibiting binding conformers similar to aricept but with better hydrogen bonding interactions with the AChE receptor, may prove to be more fruitful in yielding practical prophylactic prospects.

Finally, an important complementary method has been developed to recognize and predict prospective toxicity among covalent-binding AChE inhibitors of potential application to nerve agent prophylaxis and therapeutics. This work has recently been published in the journal Chemical Research on Toxicology, and the corresponding paper is included herein as Appendix B. While the initial work in this field focused on covalent AChE inhibitors due to a greater availability of in vivo toxicity data, modifications to the methodology are possible to extend its scope to non-covalent systems such as those reported above.

References:

1. Guo, J., Hurley, M.M., Wright, J.B., Lushington, G.H. "A Docking Score Function for Estimating Ligand-Protein Interactions: Applications to Acetylcholinesterase Inhibition." *J. Med. Chem.* 2004; **47:** 5492-5500.
2. Halgren, T.A. Merck Molecular Force Field II. MMFF94 van der Waals and Electrostatic Parameters for Intermolecular Interactions. *J. Comp. Chem.* 1996; **17:** 520-552.
3. DiverseSolutions 7.1, The Tripos Associates, Inc. St. Louis, MO, 2005
4. Stanton, D.T. Evaluation and Use of BCUT Descriptors in QSAR and QSPR Studies. *J. Chem. Inf. Comp. Sci.* 1999; **39:** 11-20.
5. Rarey M, Kramer B, Lengauer T, Klebe GJ. A Fast Flexible Docking Method using an Incremental Construction Algorithm. *J. Mol. Biol*. 1996; **261:** 470-489.

Appendix A

A Docking Score Function for Estimating Ligand−Protein Interactions: Application to Acetylcholinesterase Inhibition

Jianxin Guo,[†] Margaret M. Hurley,[‡] Jeffery B. Wright,[§] and Gerald H. Lushington*,[†]

Molecular Graphics and Modeling Lab, University of Kansas, Lawrence, Kansas 66045, U.S. Army Research Laboratory, Aberdeen Proving Ground, Maryland 21005-5067, and U.S. Army RDECOM/Natick Soldier Center, Natick, Massachusetts 01760-5020

Acetylcholinesterase (AChE) inhibition is an important research topic because of its wide range of associated health implications. A receptor-specific scoring function was developed herein for predicting binding affinities for human AChE (huAChE) inhibitors. This method entails a statistically trained weighted sum of electrostatic and van der Waals (VDW) interactions between ligands and the receptor residues. Within the 53 ligand training set, a strong correlation was found ($R^2 = 0.89$) between computed and experimental inhibition constants. Leave-one-out cross-validation indicated high predictive power ($Q^2 = 0.72$), and analysis of a separate 16-compound test set also produced very good correlation with experiment ($R^2 = 0.69$). Scoring function analysis has permitted identification and characterization of important ligand−receptor interactions, producing a list of those residues making the most important electrostatic and VDW contributions within the main active site, gorge area, acyl binding pocket, and periferal site. These analyses are consistent with X-ray crystallographic and site-directed mutagenesis studies.

Introduction

Acetylcholinesterase (AChE) is an enzyme that hydrolyzes the neurotransmitter acetylcholine (ACh) at cholinergic synapses, accomplishing its role at a rate faster than those of most other known enzymes.[1,2] Recent research interest regarding this enzyme is not only due to this high catalytic efficiency but also due to the broad implications of AChE inhibition on human health, agrochemistry, and chemical agents. For example, Alzheimer's disease (AD) is associated with low in vivo levels of acetylcholine; thus, AChE has been targeted in many drug discovery projects aimed at maintaining ACh availability via mild or reversible inhibitors such as tacrine[3] and donepezil,[4] etc. While low-level AChE inhibition is useful for such neurological treatments, higher levels of inhibition can be detrimental. Organophosphorus (OP) compounds, in particular, irreversibly deactivate AChE and may induce failure of cholinergic synaptic transmission, deterioration of neuromuscular junctions, flaccid muscle paralysis, and central nervous system seizures.[5,6] Effective drug design thus requires great care in balancing the level of inhibitive efficacy.

The availability of AChE crystal structures for various species with and without ligands provides a solid basis for structure-based design of novel AChE inhibitors.[7] There are two principle binding sites in the AChE. The catalytic active site is located at the base of a deep gorge in the enzyme. It contains a catalytic triad, Ser203, Glu334, and His447 (huAChE sequence numbering, to

be used throughout unless otherwise specified), and nearby residues (e.g., the choline binding site: Trp86) that collectively effect the ACh catalysis reactions.[8] AChE also has a peripheral anionic site (PAS) located near the enzyme surface at the mouth of the active site gorge. The residue Trp286 plays a very important role in ligand binding in the PAS. Ligand binding to the PAS affects enzymatic activity through a combination of steric blockade of ligands moving through the gorge and allosteric alteration of the catalytic triad conformation and efficiency.[9] The gorge itself is a narrow hydrophobic channel with a length of ~20 Å, connecting the PAS site to the active site.[10] An acyl binding pocket consists of residues Gly122, Trp236, Phe295, Phe297, and Phe338 and is responsible for interacting with the acetyl group.[11] Early inhibition research was mainly focused on ligands binding in the active site (e.g., tacrine[3], amiridine,[12] etc.). Recent efforts have focused on finding novel ligands that bind to both sites in order to search for more potent reversible inhibitors (e.g., TAK-147, E2020, etc.), selectively favoring the inhibition of AChE rather than the related butyrylcholinesterase (BChE).

Molecular modeling has proven increasingly important in helping to design novel enzyme inhibitors. A substantial amount of prior AChE inhibitor research has focused on using ligand-based design methods such as CoMFA.[13−17] Given an accurate receptor structure, molecular docking can also be very useful in characterizing ligand−receptor binding by providing predictions of the bound conformation for the ligand and a scheme for energetically ranking (i.e., scoring) the ligand−receptor interaction. Great successes have been achieved in terms of conformational predictions via flexible docking programs such as Dock,[18] Gold,[19] FlexX,[20] etc. Such conformational predictions are very important to drug design because (1) the binding conformation of

ligands is much easier to validate (i.e., through comparison with experimentally observed structures) than is the binding affinity for different systems and (2) the accurate prediction of the bound conformation is a prerequisite for reliable scoring. Even with good structural predictions, however, the score may not always agree well with experimentally determined affinities mainly because experimental conditions include important dynamic or entropic effects that are difficult to rigorously represent in a general scoring function. To account for such effects empirically, scoring functions are typically trained via diverse sets of previously characterized ligand–receptor interactions. Unfortunately, no finite training set is likely to provide a perfect representation for all systems of interest because of the varying physicochemical conditions present in different receptors. Indeed, with the AChE system, studies on steroidal alkaloid inhibition show no correlation between the calculated binding energy and experimentally determined activity.[21] Molecular dynamics simulations do provide a natural means for quantifying both the entropic and enthalpic components of binding affinity for ligand–AChE interactions;[20] however, extensive computational demands make molecuar dynamics (MD) simulations prohibitively time-consuming for analysis of large compound collections. In such cases, the best compromise may be to carry out simple docking studies but to explicitly train the scoring function to reproduce behavior in the system of interest. Herein, we present a new scoring function that is based on the ligand–receptor interaction field and is trained specifically to reproduce AChE inhibition.

Methods

The AChE crystal structures used herein were obtained from the Protein Databank (PDB). Our main docking and training activities have been focused on a human AChE (huAChE) structure (code, 1B41)[22] but rely on ligand binding information from a *Torpedo californica* AChE (tcAChE) structure (code, 1EVE) that includes a cocrystallized E2020 inhibitor.[23] Given the absence of a firm understanding of the persistence and roles of individual solvent molecules in and around the AChE binding sites, all waters were removed from the structures. To ascertain the orientation of the ligand E2020 relative to the huAChE structure, the huAChE structure was aligned to the tcAChE in SYBYL[24] by achieving a maximal overlap of C_α atoms for corresponding huAChE/tcAChE residues within the receptor region. The resulting root-mean square deviation (rmsd) between the two aligned huAChE/tcAChE structures is only 0.85 Å for the set of all backbone C_α atoms within the full enzyme subunit, suggesting good overall alignment and substantial structural similarity. Hydrogen atoms were added (via SYBYL) to the resulting huAChE–E2020 complex. The positions of these new protons were then optimized in MOE[25] via molecular mechanics using the MMFF94s force field[26] (all heavy atoms fixed) to avoid bad interatomic contacts. The position of E2020 was then optimized (all receptor atoms fixed) to determine a plausible stable conformational structure for the ligand in the receptor environment. In both of the above simulations, MMFF94s charges were used to account for relevant electrostatics. The

steepest descent minimization algorithm was used for the first 100 steps (unless an rms gradient of less than 100 kcal/(mol·Å) was first achieved), followed by 200 steps of conjugate gradient (unless an rms gradient of less than 1 kcal/(mol·Å) was attained), and finally completed by 1000 steps of truncated Newton (or an rms gradient of less than 0.01 kcal/(mol·Å)). The resulting E2020 structure was then extracted for subsequent docking calculations.

Sixty-nine compounds with IC_{50} data measured with human AChE assay[27–30] were selected for training and testing the scoring function. The activity among these compounds ranges from 0.33 to 30 000 nM (Tables 1 and 2). The active site for the huAChE docking calculations was constructed from the crystal structure by retaining all residues within a radius of 12 Å relative to E2020 (but discarding the original ligand itself). Docking calculations were carried out with the Gold program.[19] A genetic algorithm was used in searching the binding conformation of flexible ligands, using the default parameters in GOLD. A maximum of 20 poses were computed for each compound. Those docked conformations were saved in SDF format and then imported into SYBYL for scoring calculations according to the FlexX and CSCORE modules. The scoring methods available included empirical methods such as ChemScore,[31] FlexX score,[20] and G Score[19] and knowledge-based methods such as PMF score[32] and DrugScore.[33] Multilinear regression (MLR) was used to obtain a consensus score from these methods. One conformation was selected for each compound to give a good compromise between the best consensus score and those with the closest alignment to the original E2020 ligand. Specifically, the pose for the scoring of the activity was selected on the basis of having the highest consensus score (first criterion) and ChemScore (tie-breaking criterion), with the further stipulation that the following knowledge-based criteria (as determined by visual inspection) must be obeyed whenever possible: (1) good π–π overlap with residue Trp86, as has been found to be critical for E2020 binding;[23] (2) good π–π overlap with residue Trp286, as has also been found to be very important for E2020 complexation[23]

The chosen conformations were used to fit an interaction field whose form, basically a variant of the comparative binding energy (COMBINE) method,[34–36] is as follows:

$$pIC_{50} = \sum_i c_i E_i^{\text{ele}} + \sum_j d_j E_j^{\text{vdw}} \qquad (1)$$

where c_i and d_j are fitted coefficients, E_i^{ele} and E_j^{vdw} are electrostatic and van der Waals (VDW) interactions arising between atoms in the ith and jth residues and the ligand. In this expression, all receptor residues within 10 Å of the position of the original E2020 ligand (a total of 92 residues) were included in the summation over i, and E_i^{ele} and E_j^{vdw} were calculated via an SVL script written for the MOE system. The statistic analysis was performed in Simca-P[37] with partial least squares regression (PLS). Fifty-three of the full 69 compounds were selected as our training set, and the other 16 compounds were used as a test set for validating the predictive power of the new scoring function.
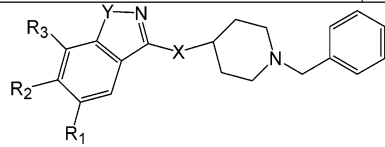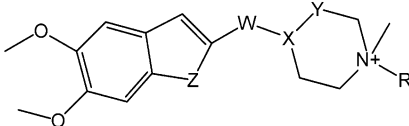
Table 1. huAChE Ligands in the Training Set

Structure					ID	IC50 (nM)	Ref	pKi exp	pKi calc

-R1	-R2	-R3	-X-	-Y-					
-H	-H	-H	-(CH$_2$)$_2$-	-O-	1	55	[28]	7.26	7.47
-CH$_3$	-H	-H	-(CH$_2$)$_2$-	-O-	2	7.8	[28]	8.11	8.05
-CH$_3$	-OCH$_3$	-H	-(CH$_2$)$_2$-	-O-	3	5.8	[28]	8.24	8.23
-OCH$_3$	-H	-H	-(CH$_2$)$_2$-	-O-	4	7.2	[28]	8.14	7.62
-H	-H	-OCH$_3$	-(CH$_2$)$_2$-	-O-	5	7.1	[28]	8.15	7.55
-H	-NH-CO-CH$_3$	-H	-(CH$_2$)$_2$-	-O-	6	2.8	[28]	8.55	8.40
-H	-NH-SO$_2$-φ	-H	-(CH$_2$)$_2$-	-O-	7	14	[28]	7.85	8.17
-H	-4-morpholino	-H	-(CH$_2$)$_2$-	-O-	8	0.8	[28]	9.10	9.23
-H	-NH$_2$	-H	-(CH$_2$)$_2$-	-O-	9	20	[28]	7.70	8.08
-H	-Br	-H	-(CH$_2$)$_2$-	-O-	10	50	[28]	7.30	7.06
-H	-CN	-H	-(CH$_2$)$_2$-	-O-	11	101	[28]	7.00	7.03
-H	-CO-NH$_2$	-H	-(CH$_2$)$_2$-	-O-	12	8.8	[28]	8.06	7.57
-H	-H	-H	-(CH$_2$)$_3$-	-O-	13	900	[28]	6.05	6.06
-H	-H	-H	-O-CH$_2$-	-O-	14	2600	[28]	5.59	5.65
-H	-H	-H	-NH-CH$_2$-	-O-	15	320	[28]	6.49	7.00
-H	-H	-H	-(CH$_2$)$_2$-	-S-	16	99	[28]	7.00	6.89
-H	-H	-H	-(CH$_2$)$_2$-	-CH=CH-	17	220	[28]	6.66	7.11
-H	-H	-H	-(CH$_2$)$_2$-	-NH-	18	120	[28]	6.92	6.82
-CH$_2$-CH$_2$-CO-NH-		-H	-(CH$_2$)$_2$-	-O-	19	0.57	[29]	9.24	8.89
-NH-CO-CH$_2$-		-H	-(CH$_2$)$_2$-	-O-	20	0.95	[29]	9.02	8.32
-N(CH$_3$)-CO-CH$_2$-		-H	-(CH$_2$)$_2$-	-O-	21	0.48	[29]	9.32	9.19
-H	-NH-CO-CH$_2$-		-(CH$_2$)$_2$-	-O-	22	3.6	[29]	8.44	8.62

-W-	-X-Y-	-Z-	-R						
-	-CH$_2$-CH-	-C(O)-	-CH$_2$-φ	23	250	[27]	6.60	6.82	
-C(O)-	-CH$_2$CH$_2$-CH-	-S-	-CH$_2$-φ	24	8	[27]	8.10	8.33	
-C(O)-	-CH$_2$C(OH)-CH-	-S-	-CH$_2$-φ	25	43	[27]	7.37	7.33	
-C(O)CH$_2$-	-C(OH)CH$_2$CH$_2$-CH-	-S-	-CH$_2$-φ	26	380	[27]	6.42	6.50	

Table 1 (Continued)
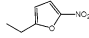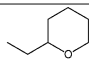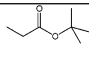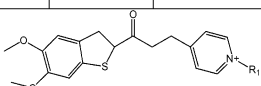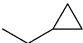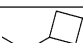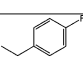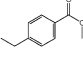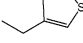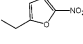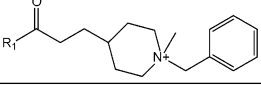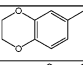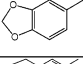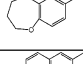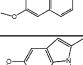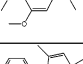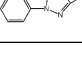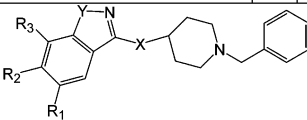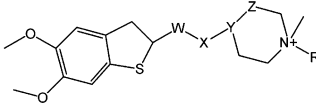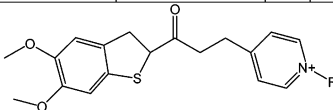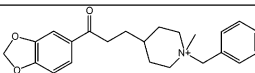
-C(O)CH$_2$-	-CH$_2$CH$_2$CH$_2$-CH-	-S-	-CH$_2$-φ	27	110	[27]	6.96	6.64
-C(O)-	-CH$_2$C(OCH$_3$)-CH-	-S-	-CH$_2$-φ	28	120	[27]	6.92	7.22
-C(O)-	-HC=C-	-S-	-CH$_2$-φ	29	520	[27]	6.28	6.90
-	-C(OH)-CH-	-S-	-CH$_2$-φ	30	19580	[27]	4.71	4.73
-	-HC=C-	-S-	-CH$_2$-φ	31	2670	[27]	5.57	5.46
-C(O)-	-CH$_2$CH$_2$-CH-	-S-	-(CH$_2$)$_2$OCH$_2$	32	53	[27]	7.28	6.89
-C(O)-	-CH$_2$CH$_2$-CH-	-S-		33	32	[27]	7.49	7.84
-C(O)-	-CH$_2$CH$_2$-CH-	-S-		34	28	[27]	7.55	7.51
-C(O)-	-CH$_2$CH$_2$-CH-	-S-		35	79	[27]	7.10	6.67
-C(O)-	-CH$_2$CH$_2$-CH-	-S-	-CH$_2$CH$_2$-O-φ	36	390	[27]	6.41	6.52
-C(O)-	-CH$_2$CH$_2$-CH-	-S-	-CH$_2$-CN	37	1000	[27]	6.00	6.06

-R1				
-CH$_3$	38	900	[27]	6.05	5.91
-CH$_2$CH$_3$	39	280	[27]	6.55	7.56
-CH$_2$CH=CH$_2$	40	540	[27]	6.27	6.66
	41	110	[27]	6.96	6.72
	42	40	[27]	7.40	7.47
-CH$_2$CH$_2$-O-CH$_2$CH$_3$	43	7	[27]	8.15	8.06
	44	2.6	[27]	8.59	8.39
	45	1000	[27]	6.00	6.07
	46	6	[27]	8.22	7.76
	47	4.5	[27]	8.35	8.33

-R1				
	48	100	[30]	7.00	7.32
	49	41.5	[30]	7.38	7.30
	50	139	[30]	6.86	6.87
	51	50	[30]	7.30	7.60
	52	120	[30]	6.92	7.61
	53	22	[30]	7.66	7.89

Table 2. Testing Set of huAChE Ligands, Showing Corresponding Inhibition Data

Structure					ID	IC50 (nm)	Ref	pKi exp	pKi pred
-R1	-R2	-R3	-X-	-Y-					
-H	-OCH$_3$	-H	-(CH$_2$)$_2$-	-O-	54	8.3	[28]	8.08	8.40
-H	-NH-CO-ϕ	-H	-(CH$_2$)$_2$-	-O-	55	9.4	[28]	8.03	7.76
-H	-OH	-H	-(CH$_2$)$_2$-	-O-	56	26	[28]	7.59	7.01
-H	-H	-H	-(CH)$_2$-	-O-	57	210	[28]	6.68	6.85
-H	-H	-H	-NH-(CH$_2$)$_2$-	-O-	58	810	[28]	6.09	7.43
-H	-H	-H	-(CH$_2$)$_2$-	-N=CH$_2$	59	340	[28]	6.47	7.06
-CH$_2$CONH-		-H	-(CH$_2$)$_2$-	-O-	60	0.33	[29]	9.48	8.18

W	X-Y-Z	-R	ID	IC50 (nm)	Ref	pKi exp	pKi pred
-C(O)-	-CH$_2$CH(OH)-CH-CH$_2$-	-CH$_2$-ϕ	61	190	[27]	6.72	6.36
-C(O)-	-CH$_2$-C(OH)-CH$_2$-	-CH$_2$-ϕ	62	90	[27]	7.05	6.41
-C(O)-	-CH$_2$-CH=CH -	-CH$_2$-ϕ	63	750	[27]	6.12	6.37
-	-CH$_2$-CH-CH$_2$-	-CH$_2$-ϕ	64	30000	[27]	4.52	5.33
-C(O)-	-(CH$_2$)$_2$-CH-CH$_2$-	-CH$_2$COOCH$_3$	65	54	[27]	7.27	6.89

-R	ID	IC50 (nm)	Ref	pKi exp	pKi pred
-(CH$_2$)$_2$CH$_3$	66	2570	[27]	5.59	5.23
-(CH$_2$)$_2$OCH$_3$	67	30	[27]	7.52	7.54
-CH$_2$-ϕ	68	4.6	[27]	8.34	8.34

	ID	IC50 (nm)	Ref	pKi exp	pKi pred
	69	240	[30]	6.62	5.76

Results and Discussion

Our scoring model built via PLS regression over interactions within the 53-molecule training set appears to be of reasonable quality, with a correlation coefficient of $R^2 = 0.89$ and a leave-one-out cross-validation correlation of $Q^2 = 0.72$. In using the scoring function to evaluate the activity of the 16-molecule testing set, we achieved good predictivity: a correlation of $R^2 = 0.69$ (Figure 1) between the calculated results and experimental values.

To compare the precision and extensibility of our scoring function, we contrasted the above results with predictions made using several commercially available scoring methods, including ChemScore,[31] FlexX score,[20] DrugScore,[33] G Score,[19] and PMF score.[32] The correlation between the experiment and any single scoring method is poor. The PMF score showed the best correlation but was still poor ($R^2 = 0.13$ for the training set). All of the other representations gave even worse correlations: ChemScore = 0.07, FlexX = 0.05, Drug-
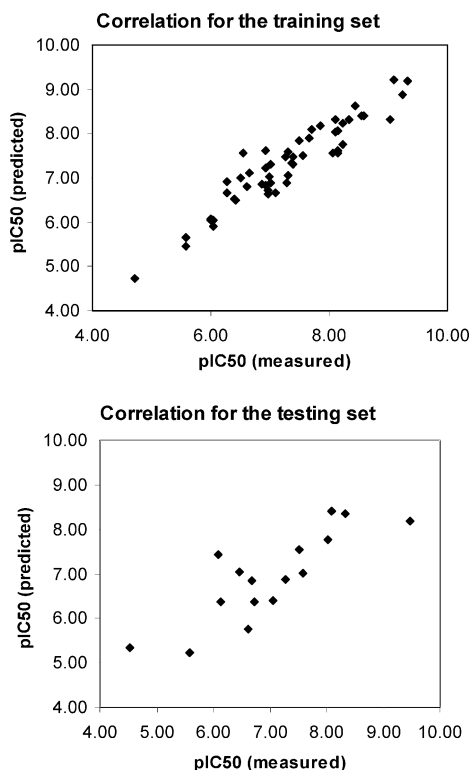
Figure 1. Correlation of the calculated activity (pIC$_{50}$) with experiment: (top) training set ($R^2 = 0.89$); (bottom) testing set ($R^2 = 0.69$).

Score = 0.01, G Score = 0.004. Since those general scoring methods were not trained in this AChE inhibition set, it is not completely fair to compare them directly with our specially tailored energy decomposition method. Therefore, we built a consensus score by training (over the 53-molecule set) a weighted sum over the above five commercially available scoring functions as follows:

$$\text{pIC}_{50} = 0.05682 \text{ Chemscore} - 0.00499 \text{ Drugscore} - 0.03582 \text{ Flexscore} - 0.01232 \text{ Gscore} + 0.01847 \text{ PMFscore} + 7.62820 \quad (2)$$

where Chemscore, Drugscore, Flexscore, Gscore, and PMFscore refer to computed affinities from the Chem-Score, DrugScore, FlexX score, G Score, and PMF score methods, respectively. Although an improvement was found for this consensus score within the training set itself ($R^2 = 0.26$), its predictive potency is poor, judging by no evident correlation within the 16-molecule testing set.

To help verify the physical sensibility of our model, we have mapped out the residues that contribute significantly to the scoring function. The coefficients of the 20 most important residues in terms of electrostatic and VDW contributions are shown in Figure 2. In those residues, Trp86, Ile451, Gly448, Tyr449, and Ser229 are the most important residues in the active site for VDW interactions. Trp86 functions by forming $\pi-\pi$ interaction with ligand aryl groups (when available), while the other residues define the shape of the gorge base, serving to discriminate according to ligand shape. In the upper gorge area and the acyl binding pocket, residues Tyr124, Phe295, Phe338, and Phe297 are responsible for providing hydrophobic contacts. The ring of Tyr72
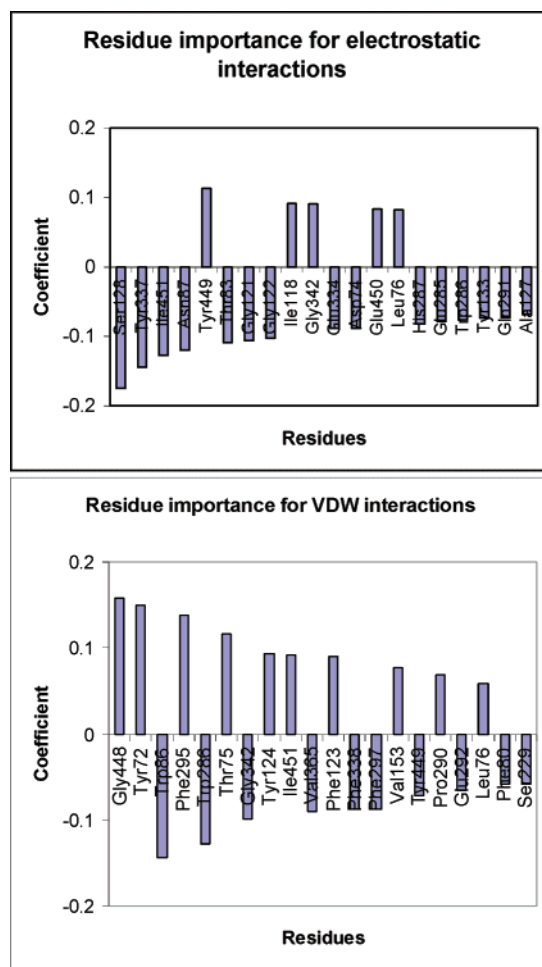

Figure 2. (Top) Coefficients of the 20 most important residues for electrostatic interactions. (Bottom) Coefficients of the 20 most important residues for VDW interactions.

is almost perpendicular to the Trp286 ring and forms a blocking wall to prevent the ligand ring from moving away from the position where it forms a $\pi-\pi$ interaction with the Trp286 ring. Phe295, Phe297, Val365, and Glu292 form another wall on the other side of the gorge, stretching from the acyl pocket toward the PAS.

Residues Tyr449, Glu450, Ile451, Ala127, Ser128, Tyr133, Ile118 near Trp86, and the "oxyanion hole" residues Gly121 and Gly122 are important in providing electrostatic interactions in the active site. Tyr337, Asp74, Thr83, and Asn87 are the primary electrostatic contributors in the gorge area. Gly342, Leu76, Glu285, Trp286, His287, and Gln291 are probably helpful in enhancing the activity of ligands with polar groups oriented in this area, as is evidenced by reports that an AChE inhibitor tethering in the position of His287 can affect the binding affinity as much as 14-fold.[38] Site-directed mutagenesis in huAChE indicated that Asp74, Tyr337, Phe338, Phe295, Phe297, Tyr133, and Glu450 can affect the affinity although it has been difficult to determine experimentally whether these residues contribute mainly electrostatic or VDW interactions.[39,40]

The docked ligand structures generally support the above analysis regarding the identity of principle residues. In our current docking calculations, molecules 2−7 all share similar conformations in the PAS. The modified groups in those molecules are actually exposed to the solvent and do not contribute directly to the ligand−
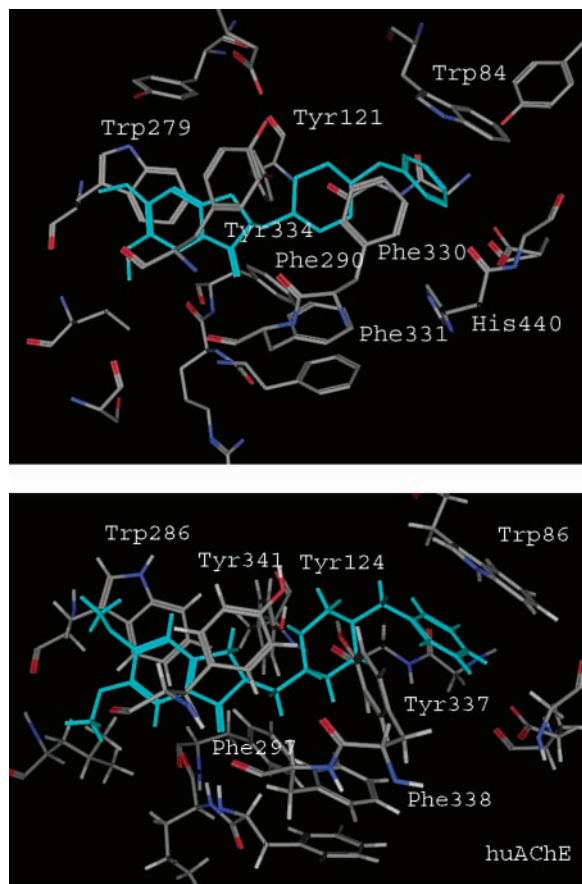
Figure 3. (Top) Structure of E2020 binding to tcAChE. E2020 is rendered in cyan. (Bottom) Structure of the E2020 binding in huAChE. E2020 is rendered in cyan.

receptor interaction. This is the same as observed in previous studies.[28] However, in the current work, molecule 8 takes a slightly different conformation with its morpholino group situating in the half-buried pocket by Trp286, His287, Ser293, Glu292, and Leu289. The morpholino oxygen has a distance of 3.65 Å from the backbone N of Glu292, and the morpholino nitrogen is 3.78 Å from the backbone O of Ser293. Such interactions could slightly pull the benzisoxazole ring away from Trp286 ring, leaving only a partial $\pi-\pi$ interaction. This particular conformation leads to an affinity increased by more than 10-fold to 0.8 nM relative to molecules 2−7. This particular region has been confirmed in an X-ray structure to be very important for the inhibitors binding to the PAS.[9]

As a final point of validation, we compared the calculated conformation for E2020 within the huAChE crystal structure relative to its original cocrystallized conformation in tcAChE. Our calculated structure suggests that E2020 has similar but not identical binding modes in tcAChE and huAChE (Figure 3). In the active site, its benzyl ring forms a $\pi-\pi$ interaction with the indole ring of Trp86 in huAChE and Trp84 in tcAChE. In the PAS, the indanone ring of E2020 forms a $\pi-\pi$ interaction with the indole ring of Trp286 in huAChE and Trp279 in tcAChE. The charged nitrogen of the E2020 piperidine ring undergoes a cation−π interaction with the phenyl ring of Phe330 in tcAChE. The corresponding residue Tyr337 in huAChE does not form a similar cation−π interaction due to the steric limitations

in this area associated with an inauspicious orientation of the Tyr337 ring. As a result, the nitrogen of the piperidine ring of the E2020 instead interacts with the hydroxyl groups of the Tyr337, Tyr124, and Ser125 within distances of 3.41, 3.12, and 4.18 Å relative to the oxygen atom of the respective hydroxyl groups. To probe the role of Tyr337, we examined the potential energy curve for Tyr337 side chain rotation relative to the other residues (energy evaluation according to the MMFF94s force field with appropriate charges) but found only one minimum in the potential curve. Closer analysis reveals that that the Tyr337 ring is trapped in a local pocket formed by Phe338, Tyr341, Trp439, Trp449, and His447. In previous structural studies and molecular dynamics simulations, it has been found that Phe330 in tcAChE can adopt a wide range of conformations in the complex structure and may function as a swinging gate[15,23,39] that structurally couples the anionic subsite of the active site and the PAS. It is natural to expect similar behavior of Tyr337 in the huAChE compared with the analogous Phe330 in tcAChE. Such a gate swing movement of the Tyr337 ring would certainly induce a shift in attached and neighboring residues; thus, one function of this PAS−active site coupling could be to effect proper residue alignment within the anionic subsite. The fact that the huAChE crystal structure used in this study to train our scoring function did not have a cocrystallized active site inhibitor (having only a PAS-bound fasciculin molecule[22]), and thus did not reflect such a conformational shift in the Tyr337, may constitute a subtle flaw in our model. Given our model's fairly strong predictive capacity, we expect the flaw to be of only minor consequence, however.

The accord between results derived from our scoring method and those of X-ray structures and mutagenesis observations indicates the effectiveness of the current analysis and the scoring function's predictive power. Since this method requires a set of compounds with known activity data to fit the score function, it is most applicable to the task of lead optimization as opposed to de novo discovery. In contrast to the comparative molecular field analysis (CoMFA)[41] method, which uses probe atoms such as nitrogen, carbon, etc. to calculate possible interaction fields between ligands and a putative receptor (and does not require explicit atomic-level representation of the receptor structure), our method uses a "real" interaction field between the ligands and receptor, thus requiring advance knowledge of the receptor structure. The benefit of using the current method is that the important residues can be directly identified and verified by site-directed mutagenesis, whereas CoMFA merely generates a hypothetical map of possible favorable and unfavorable interaction regions based on statistically postulated correlations between activity and orientations of specific functional groups within the ligand training set. Such a hypothetical map may correspond to the real interaction field if the underlying postulated statistical correlation is valid but is unlikely to be as accurate a representation as a real interaction field. In cases where crystal structures of the relevant receptor are available, CoMFA-generated hypotheses may be adjusted in order to directly correspond to the real field. In this vein, there have been successful studies that used receptor-based docking

methods to align the ligands and then used CoMFA on the resulting alignments to ascertain and analyze the resulting grid for drug design purposes.[13,14,16,17] This method is similar in principle to the COMBINE-like technique that we have applied herein to this huAChE system except that COMBINE methods are easier to compute and to understand because they only require treatment of ligand−residue interactions (hundreds of terms or less) rather than the thousands of grid points in CoMFA models. Another benefit relative to CoMFA models is that the relative simplicity of our scoring function also allows it to be used directly in any subsequent docking calculations, thus providing a means to accurately score novel inhibitor candidates and predict their bound conformations rather than having to do so in a stepwise manner.

Conclusions

A new AChE-specific scoring function has been developed herein and used in predicting binding affinity of AChE inhibitors. The method is based on a COMBINE-type approach, incorporating the electrostatic and VDW interaction fields between the ligands and receptor. A 53-compound training set was used to construct the scoring function, and a further 16 compounds were used to test the resulting model. Strong statistical correlations were found between predicted and observed affinities for both the training and testing set. Analysis of the scoring function has permitted identification of those receptor residues making the most important contributions to ligand binding. These analyses are consistent with the X-ray structure and mutagenesis studies. A comparison with other scoring methods and consensus scoring indicated the high effectiveness and predictability of this method.

Supporting Information Available: Scientific vector language (SVL) script for extracting nonbonding energy terms to compute the ligand−receptor interaction energy. This material is available free of charge via the Internet at http://pubs.acs.org.

References

(1) Taylor, P.; Radic, Z. The cholinesterases: from genes to proteins. *Annu. Rev. Pharmacol. Toxicol.* **1994**, *34*, 281−320.
(2) Massoulie, J.; Pezzementi, L.; Bon, S.; Krejci, E.; Velette, F. M. Molecular and cellular biology of the cholinesterases. *Prog. Neurobiol.* **1993**, *41*, 31−39.
(3) Crismon, M. L. Tacrine: first drug approved for Alzheimer's disease. *Ann. Pharmacother.* **1994**, *28*, 744−751.
(4) Barner, E. L.; Gray, S. L. Donepezil use in Alzheimer disease. *Ann. Pharmacother.* **1998**, *32*, p 70−77.
(5) Sidell, F. R.; Borak, J. Chemical warfare agents: II. Nerve agents. *Ann. Emerg. Med.* **1992**, *21*, p 865−871.
(6) Marrs, T. C. Organophosphate poisoning. *Pharmacol. Ther.* **1993**, *58*, 51−66.
(7) Barril, X.; Orozco, M.; Luque, F. J. Towards improved acetylcholinesterase Inhibitors: A structural and computational approach. *Mini-Rev. Med. Chem.* **2001**, *1*, 255−266.
(8) Rachinsky, T. L; Camp, S.; Li, Y.; Ekstrom, J.; Newton, M.; Taylor, P. Molecular cloning of mouse acetylcholinesterase: tissue distribution of alternatively spliced mRNA species. *Neuron* **1990**, *5*, 317−327.
(9) Bourne, Y.; Taylor, P.; Radic, Z.; Marchot, P. Structural insights into ligand interactions at the acetylcholinesterase peripheral anionic site. *EMBO J.* **2003**, *22*, 1−12.
(10) Sussman, J. L.; Harel, M.; Frolow, F.; Oefner, C.; Goldman, A.; Toker, L.; Silman, I. Atomic structure of aetylcholinesterase from *Torpedo californica*: a prototypic acetylcholine-binding protein. *Science* **1991**, *253*, 872−879.
(11) Harel, M.; Quinn, D. M.; Nair, H. K.; Silman, I.; Sussman, J. L. The X-ray Structure of a Transition State Analog Complex Reveals the Molecular Origins of the Catalytic Power and Substrate Specificity of Acetylcholinesterase. *J. Am. Chem. Soc.* **1996**, *118* (10), 2340−2346.
(12) Kojima, J.; Nakajima, K.; Ochiai, M.; Nakayama, K. Effects of NIK-247 on cholinesterase and scopolamine-induced amnesia. *Methods. Find. Exp Clin. Pharmacol.* **1997**, *19*, 245−251.
(13) Sippl, W.; Contreras, J.-M.; Parrot, I.; Rival, Y. M.; Wermuth, C. G. Structure-based 3D QSAR and design of novel acetylcholinesterase inhibitors. *J. Comput.-Aided Mol. Des.* **2001**, *15*, 395−410.
(14) Sippl, W. Development of biologically active compounds by combining 3D QSAR and structure-based design methods. *J. Comput.-Aided Mol. Des.* **2002**, *16*, 825−830.
(15) Kua, J.; Zhang, Y.; Mccammon, J. A. Studying enzyme binding specificity in acetylcholinesterase using a combined molecular dynamics and multiple dockign approach. *J. Am. Chem. Soc.* **2002**, *124*, 8260−8267.
(16) Bernard, P.; Kireev, D. B.; Chretien, J. R.; Fortier, P.-L.; Coppet, L. Automated docking of 82 *N*-benzylpiperidine derivatives to mouse acetylcholinesterase and comparative molecular field analysis with natural alignment. *J. Comput.-Aided Mol. Des.* **1999**, *13*, 355−371.
(17) Cho, S. J.; Garsia, M. L. S.; Bier, J.; Tropsha, A. Strucutre-Based Alignment and Comparative Molecular Field Analysis of Acetylcholinesterase Inhibitors. *J. Med. Chem.* **1996**, *39*, 5064−5071.
(18) Kuntz, I. D.; Blaney, J. M.; Oatley, S. J.; Langridge, R.; Ferrin, T. E. A geometric approach to macromolecule−ligand interactions. *J. Mol. Biol.* **1982**, *161*, 269−288.
(19) Jones, G.; Willett, P.; Glen, R.; Leach, A. R.; Taylor, R. Development and Validation of a Genetic Algorithm for Flexible Docking. *J. Mol. Biol.* **1997**, *267*, 727−748.
(20) Rarey M.; Kramer, B.; Lengauer, T.; Klebe, G. J. A fast flexible docking method using an imcremental constructuion algorithm. *J. Mol. Biol.* **1996**, *261*, 470−489.
(21) Haq, Z.-U.; Wellenzohn, B.; Liedl, K. r.; Rode, B. M. Molecular docking studies of Natural Cholinesterase Inhibiting Steroidal Alkaloids from *Sarcococca saligna*. *J. Med. Chem.* **2003**, *46*, 4087−4090.
(22) Kryger, G.; Harel, M.; Giles, K.; Toker, L.; Velan, B.; Lazar, A.; Kronman, C.; Barak, D.; Ariel, N.; Shafferman, A.; Silman, I.; Sussman, J. L. Structure of Recombinant Native and E202Q Mutant Human Acetylcholinesterase Complexed with the Snake-Venom Toxin Fasciculin-II. *Acta Crystallogr., Sect. D* **2000**, *56*, 1385−1394.
(23) Kryger, G.; Silman, I.; Sussman, J. L. Structure of acetylcholinesterase complexed with E2020(Aricept): implications for the design of new anti-Alzheimer drugs. *Struct. Fold Des.* **1999**, *7*, 297−307.
(24) *Sybyl/Unity*, version 6.9; Tripos Inc.: St. Louis, MO, 2002.
(25) *Molecular Operating Enviroment (MOE) 2002.03*; Chemical Computing Group Inc., Montreal, Quebec, Canada, 2002.
(26) Halgren, T. A. MMFF VI. MMFF94s Option for Energy Minimization Studies. *J. Comput. Chem.* **1999**, *20*, 720−729.
(27) Palin, R.; Clark, J. K.; Cowley, P.; Muir, A. W.; Pow, E.; Prosser, A. B.; Taylor, R.; Zhang, M.-Q. Novel Piperidinium and Pyridinium Agents as Water-Soluble Acetylcholinesterase Inhibitors for the Reversal of Neutomuscular Blockade. *Bioorg. Med. Chem. Lett.* **2002**, *12*, 2569−2572.
(28) Villalobos, A.; Blake, J. F.; Biggers, C. K.; Butler, T. W.; Chapin, D. S.; Chen, Y. L.; Ives, J. L.; Jones, S. B.; Liston, D. R.; Nagel, A. A.; Nason, D. M.; Nielsen, J. A.; Shalaby, I. A.; White, W. F. Novel Benzisoxazole Derivatives as Potent and Selective Inhibitors of Acetylcholinesterase. *J. Med. Chem.* **1994**, *37*, 2721−2734.
(29) Villalobos, A.; Butler, T. W.; Chapin, D. S.; Chen, Y. L.; Demattos, S. B.; Ives, J. L.; Jones, S. B.; Liston, D. R.; Nagel, A. A.; Nason, D. M.; Nielsen, J. A.; Ramirez, A. D.; Shalaby, I. A.; White, W. F. 5,7-Dihydro-3-[2-[1[(phenylmehtyl)-4-piperidinyl]-ethyl]-6*H*-pyrrolo[3,2-*f*]-1,2-benzisoxazol-6-one: A Potent and Centrally-Selective Inhibitor of Acetylcholinesterase with an Improved Margin of Safety. *J. Med. Chem.* **1995**, *38*, 2802−2808.

(30) Clark, J. K.; Cowley, P.; Muir, A. W.; Palin, R.; Pow, E.; Prosser, A. B.; Taylor, R.; Zhang, M.-Q. Quaternary Salts of E2020 Analogues as Acetylchoinesterase Inhibitors fo rthe Reversal of Neuromuscular Block. *Bioorg. Med. Chem. Lett.* **2002**, *12*, 2565−2568.

(31) Eldridge, M. D.; Murray, C. W.; Auton, R. R.; Paolini, G. V.; Mee, R. P. Empirical scoring functions: I. The development of a fast empirical scoring function to estimate the binding affinity of ligands in receptor complexes. *J. Comput.-Aided Mol. Des.* **1997**, *11*, 425−445.

(32) Muegge, I.; Martin, Y. C. A general and fast scoring function for protein−ligand interactions: a simplified potential approach. *J. Med. Chem.* **1999**, *42*, 791−804.

(33) Gohlke, H.; Hendlich, M.; Klebe, G. Predicting Binding Modes, Binding Affinities and "Hot Spots" for Protein−Ligand Complexes Using a Knowledge-Based Scoring Function. *Perspect. Drug Discovery Des.* **2000**, *20*, 115−144.

(34) Wang, T.; Wade, R. C. Comparative binding energy (COMBINE) analysis of OppA−peptide complexes to relate structure to binding thermodynamics. *J. Med. Chem.* **2002**, *45* (22), 4828−4837.

(35) Kmunicek, J.; Bohac, M.; Luengo, S.; Gago, F.; Wade, R. C.; Damborsky, J. Comparative binding energy analysis of halo-alkane dehalogenase substrates: modelling of enzyme−substrate complexes by modelcular docking and quantum mechanical calculations. *J. Comput.-Aided Mol. Des.* **2003**, *17* (5−6), 299−311.

(36) Murcia, M.; Ortiz, A. R. Virtual screening with flexible docking and COMBINE-based models. Appliction to a series of factor Xa inhibitors. *J. Med. Chem.* **2004**, *47* (4), 805−820.

(37) *SIMCA-P*; Umereics AB, Umea, Sweden, 2001.

(38) Shafferman, A.; Velan, B.; Ordentlich, A.; Kronman, C.; Grosfeld, H.; Leitner, M.; Flashner, Y.; Cohen, S.; Barak, D.; Ariel, N. Substrate inhibition of acetylcholinesterase: residues affecting signal transduction from teh surface to the catalytic center. *EMBO J.* **1992**. *11*, 3561−3568.

(39) Johnson, J. L.; Cusack, B.; Hughes, T. F.; Mccullough, E. H.; Fauq, A.; Romanovskis, P. R.; Spatola, A. F.; Rosenberry, T. L. Inhibitors tethered near the acetylcholinesterase active site serve as molecular rulers of the peripheral and acylation sites. *J. Biol. Chem.* **2003**, *278*, 38948−38955.

(40) Ordentlich, A.; Barak, D.; Kronman, C.; Ariel, N.; Segall, Y.; Valan, B.; Shafferman, A. The architecture of human acetylcholin-esterase active center probed by interactions with selected organophosphate inhibitors. *J. Biol. Chem.* **1996**, *271*, 11953−11962.

(41) Cramer, R. D., III; Petterson, D. E.; Flume, J. D. Comparative Molecular Field Analysis (CoMFA). 1. Effect of Shape on Binding of Steroids to Carrier Proteins. *J. Am. Chem. Soc.* **1988**, *110*, 5959−5967.

Appendix B

Mechanistic Insight into Acetylcholinesterase Inhibition and Acute Toxicity of Organophosphorus Compounds: A Molecular Modeling Study

Jian-Xin Guo,[†] Jay J.-Q. Wu,[⊥] Jeffery B. Wright,[‡] and Gerald H. Lushington*,[†]

Molecular Graphics and Modeling Lab, University of Kansas, Lawrence, Kansas 66045, VM Discovery, Inc., Fremont, California 94538, and U.S. Army RDECOM/Natick Soldier Center, Natick, Massachusetts 01760

Acute toxicity of organophosphorus (OP) compounds results mainly from irreversible acetylcholinesterase (AChE) inhibition; however OP toxicity frequently hinges on prior biotransformations that produce toxic metabolites. To account for both precursor metabolic effects and primary AChE inhibition, we included absorption, distribution, metabolism, excretion (ADME) effects, ligand binding, and reactive AChE phosphorylation and aging in a detailed but computationally expedient phenomenological toxicity model. Ligand negative accessible surface area (NASA) was used as a generic ADME descriptor, while relevant metabolic, phosphorylation, and aging reactions were assessed via quantum chemical enthalpy calculations, and the binding affinity of the Michaelis complex was quantified via Comparative Molecular Field Analysis (CoMFA). The resulting model correlates very well ($R^2 = 0.90$) with experimental acute toxicity measurements and provides useful mechanistic insight into the underlying toxicity. Model predictivity was validated by leave-one-out cross-validation ($Q^2 = 0.82$). The Michaelis binding affinity descriptor has the largest weight in our model, but subsequent covalent inhibition and prior ADME effects also exhibit significant effects.

Introduction

Organophosphorus (OP) compounds are best known for their highly toxic effect as agricultural chemicals and chemical warfare agents. The mechanism of the acute OP toxicity has been a subject of substantial research interest for several decades in the search for therapies to counter OP poisoning (e.g., oximes (*1*)), to devise more effective pesticides, and to uncover low-toxicity OP species for potential pharmacological applications (*2*). The main cause of OP toxicity is irreversible inhibition of the acetylcholinesterase (AChE) enzyme (*2*). AChE hydrolyzes the neurotransmitter acetylcholine (ACh) at cholinergic synapses. The inactivation of the AChE by OP compounds thus causes acetylcholine buildup, which can in turn induce failure of cholinergic synaptic transmission, leading to deterioration of neuromuscular junctions, flaccid muscle paralysis, and central nervous system seizures (*3*, *4*).

Numerous studies via a number of different techniques (e.g., crystallography (*5*), mutagenesis (*6*), modeling (*7*), etc.) concur that OP compounds mainly interact with the AChE catalytic triad (residues Ser203, His447, and Glu334 according to the mouse AChE sequence) in the active site, which is connected by a deep narrow gorge to the peripheral binding site at the entrance of the enzyme. The inhibition mechanism involves phosphorylation whereby a covalent bond between the central phosphorus atom of the ligand and the side chain oxygen of Ser203 is formed. For some OP compounds, the resulting conjugate can further react via a process known as "aging" that usually involves the loss of an alkyl group from the phosphyl alkoxy substitutent. The aging process prevents AChE reactivation by conventional antidotes such as oxime therapy.

Many OP compounds do not interact with AChE in vivo in their native form. The metabolite products, usually oxon analogues, are frequently the actual toxicants (*8*). The usual metabolism reactions include oxidative desulfuration, N-dealkylation, O-dealkylation, O-dearylation, thioether oxidation, among others (*9*). It is thus not surprising that in vitro inhibition measurements rarely provide a simple linear correlation with the acute toxicity. To better understand the mechanism of OP activity, it is necessary to augment information from direct AChE inhibition studies with an account of absorption, distribution, metabolism, and excretion (ADME) processes. Given such complex underlying biological processes, a full investigation and understanding of the uptake and toxicology of even a single OP compound can make for a daunting experimental challenge.

Molecular modeling methods have been very useful in helping to understand OP toxicity because of the complexity of the AChE system and the arduous, expensive, and sometimes dangerous nature of the corresponding experiments. Previous modeling studies have largely focused on the direct inhibition of AChE, mainly by probing the interaction of ligands with the AChE active site (*10*). Those methods include quantum chemistry (*7*), molecular dynamics (*7*), docking (*11*), and interaction field analysis of noncovalent ligands (*12*). In the present paper, we will focus on a detailed but computationally efficient scheme for integrating ADME properties, AChE binding affinity, phosphorylation, and the aging process into a single, unified, phenomenological model capable of reproducing the primary trends in OP toxicity in a mechanistically intuitive fashion.

Materials and Methods

Inhibitors. Data corresponding to the 38 OP compounds considered for this study are listed in Table 1. The LD_{50} values correspond to studies on male rats exposed orally and are given in mg/kg body weight. Among those compounds, Dichlorvos, Dicrotophos, Naled, Tetrachlorvinphos, Ethoprop, Oxydemeton-methyl,

* To whom correspondence should be addressed. Tel: +1-785-864-1140. Fax: +1-785-864-5326. E-mail: glushington@ku.edu.

† University of Kansas.

⊥ VM Discovery, Inc.

‡ U.S. Army RDECOM/Natick Soldier Center.

Table 1. Organophosphorus Compounds Considered for Analysis[a]

parent	metabolite	direct acting	metabolite references	LD$_{50}$[b] (mg/kg)	pLD$_{50}$[c]
Dichlorvos		yes		80	4.097
Dicrotophos		yes		21	4.678
Naled		yes		250	3.602
Tetrachlorvinphos		yes		4000	2.398
Trichlorfon	Dichlorvos	no	31	650	3.187
Ethoprop		yes		34	4.469
Azinphos Methyl	oxon	no	32	13	4.886
Bensulide	?	no		770	3.113
Dimethoate	oxon	no	33	215	3.668
Disulfoton	?	no		2	5.699
Ethion	oxon	no	34	13	4.886
Malathion	oxon	no	35	1375	2.862
Methidathion	oxon	no	36	31	4.509
Phorate	oxon	no	37	2	5.699
Phosmet	oxon	no	38	147	3.833
Sulfopros	oxon	no	39	65	4.187
Temephos	?	no		8600	2.066
Terbufos	oxon	no	41	2	5.699
Fonofos	oxon	no	41	3	5.523
Oxydemeton-methyl		yes	42	47	4.328
Profenofos		yes	43	358	3.446
Chlorethoxyfos	?	no		5	5.301
Chlorpyrifos	oxon	no	44	155	3.810
Coumaphos	oxon	no	45	41	4.387
Diazinon	oxon	no	46	250	3.602
Fenitrothion	oxon	no	47	740	3.131
Fenthion	oxon	no	48	215	3.668
Methyl Chlorpyrifos	oxon	no	49	1500	2.824
Methyl parathion	oxon	no	50	14	4.854
Parathion	oxon	no	51	13	4.886
Pirimiphos methyl	oxon	no	52	1450	2.839
Sulfotep	?	no		5	5.301
Tebupirimphos	?	no		2	5.699
Fenamiphos		yes		8	5.097
Acephate	?	no		700	3.155
Methamidophos		yes		31	4.509
Isofenfos	oxon	no	53	28	4.553
Propetemphos	?	no		119	3.924

[a] The compounds with question mark in the metabolite were not used in the current work. [b] The data are from ref 8. [c] The pLD$_{50}$ was calculated as $6 - \log(LD_{50})$.

Profenofos, Fenamiphos, and Methamidophos all have direct interaction with AChE, while the other 29 undergo biotransformation before reaching the AChE active site. Unfortunately, to the best of our knowledge, there are no conclusive metabolic data available in the literature for Bensulide, Disulfoton, Temephos, Chlorethoxyfos, Sulfotep, Tebupirimphos, Acephate, and Propeteamphos. Based on data availability, we thus chose a total of 30 OP compounds (9 direct-acting and 21 indirect-acting species for which definitive metabolic data exists) for further analysis.

Receptor Model. The following AChE crystal structures were obtained from protein data bank (*13*) and used as structural references in this study: (1) *Torpedo californica* AChE with nerve agent VX after phosphorylation (1VXR) (*14*), (2) *Torpedo californica* AChE with nerve agent VX after aging (1VXO) (*14*), and (3) mouse AChE complexed with Gallamine (1N5M) (*15*). The latter structure, with Gallamine removed, was used as a template for assembling our ligand–receptor complex models. Since rat AChE is highly similar to mouse AChE (only 11 amino resides difference between the two (*16*), with none of those 11 playing any known role in the enzymatic activity or inhibition), we expect no appreciable difference in result to arise from using the mouse rather than the rat structure. All water and heteroatoms were removed from the structure before adding hydrogen atoms. Protein electrostatics were modeled via AMBER94 charges (*17*), and MMFF94 charges (*18*) were employed for ligands. The 1VXR and 1VXO structures served as guides for positioning inhibitors within the AChE structure. Both 1VXR and 1VXO were superimposed with 1N5M to determine (by analogy to the cocrystallized VX) positions of the ligands in pro-aging and post-aging by methods that have been described in a previous study on noncovalent inhibitors (*12*).

Descriptors. Given a focus on developing a mechanistically insightful phenomenological model, descriptors were chosen according to a requirement of having a natural physicochemical relationship with the various physiological effects under consideration (ADME processes, noncovalent complex formation, and covalent reactivity). For reasons elaborated on in the coming sections, ADME effects were modeled via ligand negative accessible surface area (NASA; as computed via the MOE suite of software (*19*) using default settings and MMFF94 charges (*18*)) plus thermochemical characterization of the associated metabolic reaction, noncovalent binding was approximated via a CoMFA model, and trends among covalent enzymatic and inhibitive processes were modeled via their thermochemistry. All thermochemical quantification was done via quantum mechanically computed molecular energies. To strike a balance between computational efficiency and reliable representation of energetic trends among our ligands, quantum chemical calculations were carried out at the AM1 level (*20*) using MOPAC7 (*21*). The MMFF94 force field (*18*) was used in the various nonquantum chemical molecular modeling calculations. Conformation searches were performed using a stochastic method similar to the RIPS method (*22*). Ligand alignment for the CoMFA model was determined by a pharmacophore-driven flexible alignment method within MOE (*19*). In the interaction field calculations, a monoanionic oxygen anion was used as probe atom to calculate the energy on a grid at intervals of 1 Å. Both electrostatic and van der Waals interaction energies were saved at each grid point for further partial least-squares (PLS) analysis via the Simca-P software (*23*).

Results and Discussion

Metabolic Effects. OP compounds may be biotransformed by many of the different cytochrome P450 isozymes. For example, CYP2C11, CYP3A4, and CYP2B1/2 were recently identified as playing a role in rat metabolism of diazinon (*9*). At this current stage, there is little information on which specific isozyme accomplished the metabolism of each specific OP compounds. In general, the reaction rate of the biotransformation should be determined largely by the reaction barrier of the corresponding P450 enzymatic reaction. Theoretically, these barriers could be accurately quantified via high-level quantum mechanical transition state calculations, however such a computationally demanding undertaking is not realistic given the number of OP compounds to be studied and the inherent structural complexity of enzymatic reactions, not to mention the frequent lack of information regarding the specific P450 isozyme responsible for metabolizing a given compound. However, it is substantially easier to identify and characterize specific metabolites rather than the intervening transition states. As a simple approximation, we thus consider the underlying thermochemistry, energetically characterizing both the initial and final states for the biotransformation, since those two states do carry important information about the viability and propensity of a given biotransformation. All relevant initial and final state compounds are listed in Table 1, under the "parent" and "metabolite" columns, respectively. All of the toxic OP compounds listed in Table 1 were identified from a literature search on rat OP toxicology. Most of the metabolites take the form of the corresponding OP–oxon. Trichlorfon has been biotransformed as Dichlorvos, which itself can have a direct interaction with AChE. Interestingly, Trichlorfon has a LD$_{50}$ of 8 times greater than its metabolite Dichlorvos, a difference likely reflecting the dilutional effects of the biotransformation.

Molecular Surface Area. The surface area has been found to play important roles in various ADME processes for central nervous system drugs, including effects on membrane transport (*24*), Caco-2 permeability (*25*), and blood–brain barrier transit (*26*), among others. Since the negative and positive surfaces
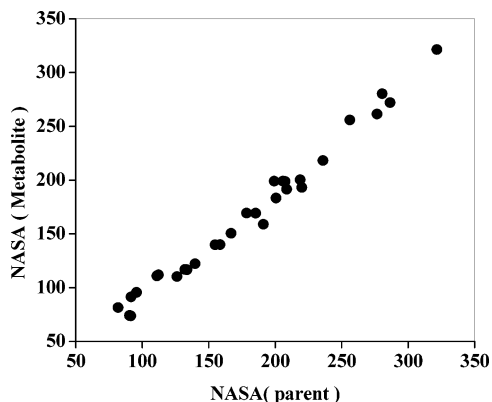
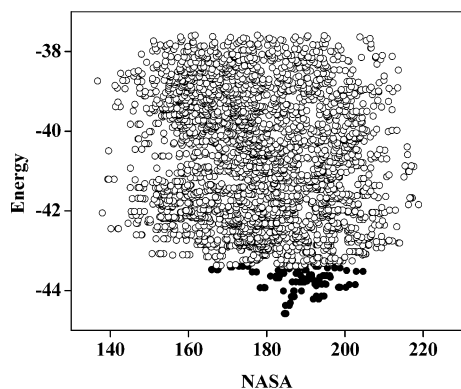**Figure 1.** Correlation of the negative polar surface area between parent OP and its metabolite.

Figure 2. Energy and surface area of the 3000 conformations for ethion. The filled circles indicate the 100 conformations with lowest energy.

play different roles in the ADME properties, it is necessary to deal with them separately. In OP compounds, one of the most obvious distinguishing structural characteristics is the distribution of negative charge in the shell around the phosphate, phosphonate, or phosphinate group. Consequently, we have selected the negative accessible surface area (NASA) as a primary descriptor to account for the ADME properties of OP compounds. Since both the parent OP and its metabolite undergo some distribution and transportation, these properties should be considered for estimating ADME properties. We compared the NASA between parent OP compounds and their metabolites (lowest energy conformations in each case) and report the results in Figure 1. A strong correlation ($R^2 = 0.98$) is observed between parent and metabolite NASA, which is not surprising because the OP−oxon form of most of the metabolites is highly similar to the parent structure. In this regard, NASA values derived from either the parent OP or its metabolite are equally suitable for estimating ADME effects.

Since NASA values depend on the molecular conformation, it is necessary to take into account any conformation change that may result from constituent steps in the ADME process. Conformational flexibility is related to the number of the rotatable bonds within a molecule. In the 30 OP compounds, the number of rotatable bonds ranges from 5 for methamidophos to 16 for ethion. Across a spread of 3000 distinct conformations of ethion (Figure 2), the NASA varies by at most 20%; however, in the 100 conformations with lowest energy, the difference is less than 10%. Apparently, the NASA dependence on conformation is relatively small and is further narrowed by energy-delimited restraints. We believe, therefore, that it is reasonable to use the lowest-energy conformation as our basis for calculating ADME properties in the current study.

A QSAR model for LD_{50} based on ADME descriptors alone yields a correlation of only $R^2 = 0.26$, and a root-mean-square error of rmse = 0.74. This indicates that substantial discrimination among OP toxicants arises from issues relating to their direct interactions with AChE.

Phosphorylation. Once OP compounds access the active site of AChE, they generally first form a covalent bond between the active serine by nucleophilic attack. The transient complex then forms a stable tetrahedral adduct after expelling a leaving group and, thus, completes the phosphorylation process. Similar to the case for OP metabolism, it is impractical to do high-level quantum chemical transition state calculations for all of the OP compounds in order to rigorously predict the activation energy barrier and corresponding reaction rate. We thus, once again, approximate the relative propensity of a given reaction by evaluating its enthalpy as a function of the initial and final states. Note that the basic structure of the AChE active site prior to OP binding does not vary as a function of the OP itself and thus can be eliminated as a constant across the set of different OP species. Consequently, for our thermochemical evaluation of the reactant state, we have restricted ourselves to quantum chemical modeling of the OP compounds alone, whereas our model approximated the product state via an OP−Ser203 conjugate. In each case, the energy corresponded to that of an AM1-optimized geometry.

Ligand Aging. The phosphorylated conjugate can, in some cases, proceed to the aging step and thus complete an irreversible enzyme inhibition. In general, the aging involves departure of the alkyl group from the phosphyl alkoxy substituent in the conjugate. In a recent study on nerve agent Tabun, however, it has been found that aging occurs through the scission of the P−N bond rather than scission of the O−C bond, although both bonds exist in the agent (*27*). Fenamiphos, Methamidophos, and Isofenphos all have functional group similar to Tabun and thus should probably also undergo scission of the P−N bond in the aging process. The initial reactant state for aging is the Ser203−OP conjugate, and the product is the Ser203−OP-aged conjugate plus the departed aging leaving group, both of which have been energetically evaluated for each OP compound again via AM1 optimizations. Considering all of these issues in addition to the previously defined metabolic parameters allows us to derive the following relationship:

$$pLD_{50} = 2.82 - 0.001\ 42E(\text{orig}) + 0.0312E(\text{met}) - (0.004\ 95)(\text{NASA}) - 0.0364E(\text{s203op}) - 0.0249E(\text{plg}) + 0.005\ 85E(\text{s203op\_aged}) - 0.0290E(\text{alg}) \quad (1)$$

where $E(\text{orig})$ is the energy of the parent OP compound, $E(\text{met})$ is the energy of the metabolite compound, NASA is the negative accessible surface area of the metabolite compound, $E(\text{s203op})$ is the energy of the Ser203-OP compound, $E(\text{plg})$ is the energy of the phosphorylation leaving group, $E(\text{s203op\_aged})$ is the energy of the aged Ser203−OP compound, and $E(\text{alg})$ is the energy of the aging leaving group. This equation results in a correlation score ($R^2 = 0.49$; rmse = 0.62) (Figure 3) that is improved relative to models derived on ADME considerations alone but is still of only borderline statistical significance. It is likely that better correlation could be achieved by augmenting the above expression with terms from the voluminous existing descriptor libraries; however, it is our desire to avoid overfitting the expression with quantities that may not provide obvious mechanistic insight. Indeed, having seven descriptors in eq 1 already runs some risk of overfitting, although, mechanistically, it is difficult to argue for the omission of any of them. The intuitively reasonable way of improving the above model is to
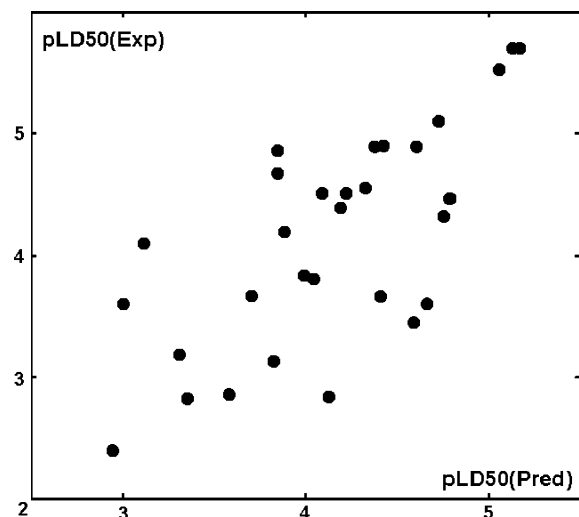
Figure 3. Correlation between experimental pLD$_{50}$ and the prediction from eq 1.

account for noncovalent precursor (Michaelis) binding complex formation between the ligand and enzyme prior to phosphorylation—a key to many inhibition processes and likely an important discriminating factor in the AChE inhibition process.

Subsite Binding Effects. The AChE gorge region is a biochemically complex construct with numerous subsites playing roles in the normal enzymatic function and ultimately also in the inhibition process. The AChE subsites that play roles in the binding of OP compounds include (a) the esteratic site containing the active site serine; (b) the "oxyanion hole" consisting of residues Gly121, Gly122, and Ala204; (c), the "anioinic subsite" or the choline binding subsite, Trp86; (d) the hydrophobic site for the alkoxy leaving group of the substrate containing an "aromatic patch" that includes resides Trp86, Tyr337, and Phe338; and (e) the acyl pocket, Phe295 and Phe297 (*28*). Normally, one would address the binding affinity by simply computing the interaction energy between OP and AChE. However, at the current stage, (a) the extent and complexity of the AChE active site render such calculations impractical at the quantum chemical level for such a number of OP compounds and (b) no docking programs are capable of reliably representing the formation of covalent bonds. Instead, we have chosen to characterize affinity trends herein via Comparative Molecular Field Analysis (CoMFA).

The most important step in CoMFA is to obtain molecular conformations that correspond reasonably well to those observed for each ligand in its bound state. In previous investigations, it has been concluded that the phosphorylation conjugate should have the P=O oriented to the oxyanion hole to take advantage of available hydrogen bonding (*28*). Furthermore, the P−OR moiety should be oriented in a manner that permits His447 imidazolium involvement in the aging. Such advance knowledge is of great value in assembling reasonable OP conformers for the CoMFA and in interpreting the eventual results. In the current work, all OP metabolites were aligned to the crystal structure of postphosphorylation VX. In the first step of the alignment, the phosphorus center was aligned with the VX phosphorus in 1VXR to determine the anchor point within the receptor active site. Once the phosphorus aligned correctly, the P was fixed in place to permit rapid alignment of the rest of the molecule. Flexible alignment was done by weighting the pharmacophore feature of each atom with a Gaussian function. The aligned structures are shown in Figure 4. It is apparent from the structural overlap that the phosphorylation leaving group

has more flexibility than the other functional groups. This seems reasonable given that the relatively small space near the Ser203, His447, and acyl pocket in the active site likely restrains the P=O and the aging leaving group but does not impinge on the phosphorylation leaving group.

To generate our CoMFA model, an oxygen anion probe was used to calculate the interaction energy at grid points. Our CoMFA methodology was fairly conventional in that we used both electrostatic and van der Waals interactions to quantify the energy. This resulted in 28 392 data points for each of the 30 compounds. After filtering those nonsignificant terms according to a variable importance threshold of 0.8, we were left with 2586 data points for each compound on which to perform the PLS regression. One principle component was used. The resulting correlation between predicted AChE binding affinity and experiment pLD$_{50}$ value, shown in Figure 5, gave $R^2 = 0.892$, with a leave-one-out cross-validation score of $Q^2 = 0.571$. The corresponding rmse was 0.3, and the F value was 111.804. The CoMFA results reveal that the electrostatic effect is more important (fraction of 0.657) than the steric effect (0.343).

To further analyze the spatial distribution of favorable and unfavorable interactions between AChE and the OP compounds, the molecular surface was plotted (Figure 6) as a function of all aligned OP metabolites. The molecular surface shown was calculated as the isosurface of the zero van der Waals potential. Regions predicted to be exposed are shown in blue, hydrophilic interactions in red, and hydrophobic in gray. This molecular surface is consistent with the structure of the active site and the known OP/AChE inhibitive mechanism. The red region near the P=O group indicates strong negative electrostatic potential, which corresponds to probable hydrogen bonding within the oxyanion hole (primarily Gly121 and Gly122). The field near P−OR suggests a possible interaction with His447 in that the gray regions near the terminal alkyl group indicate favorable hydrophobic interactions. The mixed red, gray, and blue region around the phosphorylation leaving group indicates access to a relatively large space and dynamic multigroup interactions. The major force governing the orientation of the phosphorylation leaving group is likely a hydrophobic interaction toward Trp86 and the entrance of the gorge.

To further explore the OP inhibition of AChE, we also studied the interaction between the phosphorylated OP moiety and the AChE receptor. The net electrostatic and van der Waals interaction energies were tested for direct correlation with acute toxicity; however, no statistically significant relationship was found. As a result, we have concluded that the actual AChE OP inhibition process is mainly governed by the binding energy of the Michaelis complex and the relative propensity of the phosphorylation and aging processes.

Unified Model. To best predict the acute toxicity of the OP compounds, we have integrated the results of the CoMFA model with those of the thermochemical and ADME analyses to arrive at the following relationship:

$$\begin{aligned} \text{pLD}_{50} = &-0.722 - (1.30 \times 10^{-4})(E(\text{orig})) - \\ &1.6310^{-3}E(\text{met}) - (5.00 \times 10^{-5})(\text{NASA}) - \\ &(3.60 \times 10^{-3})(E(\text{s203op})) + (2.91 \times 10^{-3})(E(\text{plg})) + \\ &(5.40 \times 10^{-4})(E(\text{s203op\_aged})) - (4.87 \times 10^{-3})(E(\text{alg})) + \\ &(0.985)(\text{CoMFA}) \quad (2) \end{aligned}$$

where the CoMFA term is the calculated affinity score from the molecular interaction field. Although the CoMFA term clearly dominates the overall eq 2 and little improvement is noted in the primary correlation ($R^2 = 0.90$; rmse = 0.301; F
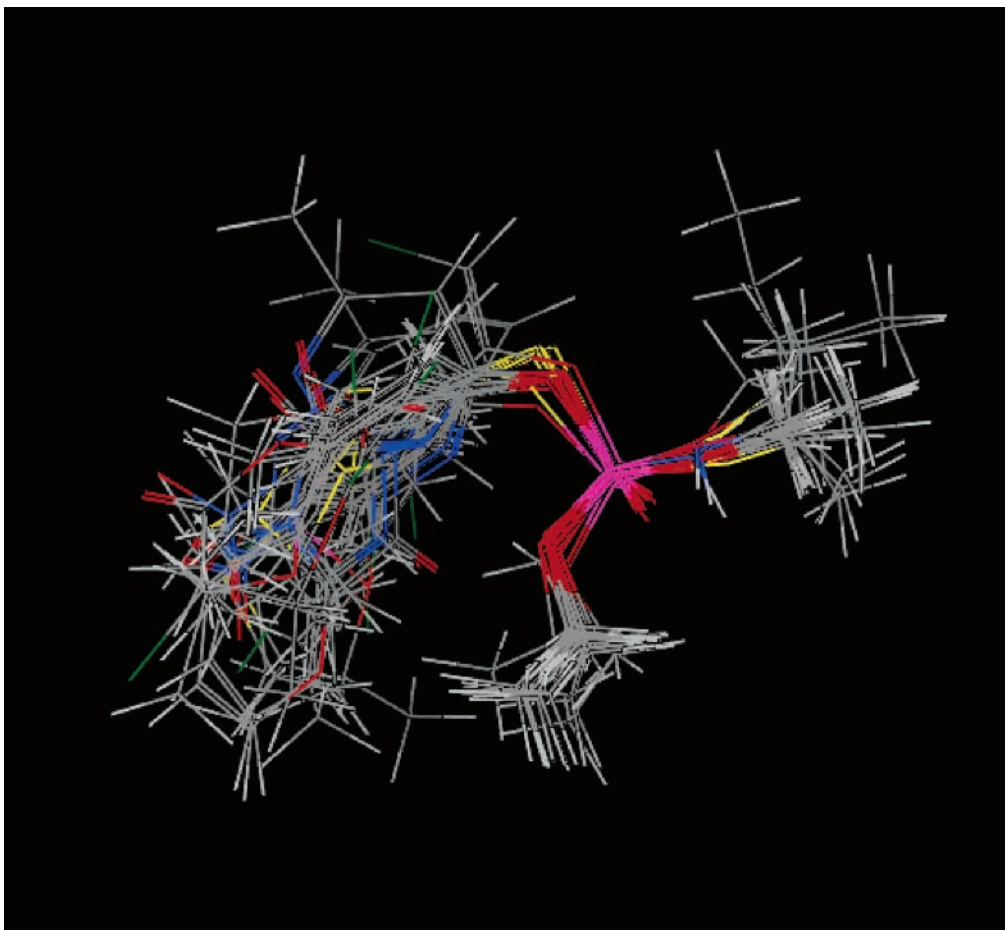
Figure 4. Aligned structures of the 30 OP metabolites. Oxygen in red, carbon in gray, sulfur in yellow, nitrogen in blue, and hydrogen in white.
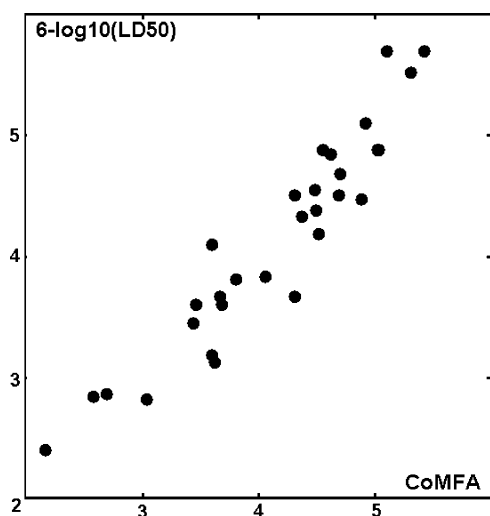

Figure 5. Correlation between experimental pLD_{50} and the predicted CoMFA score.

= 45.137; see Figure 7), the fully integrated model enjoys better predictivity than either the CoMFA alone or the phenomenological expression (eq 1) that it complements, with a cross-validated correlation of $Q^2 = 0.82$. The strong cross-validated correlation suggests good internal consistency that would not be possible with overfitting and, thus, validates our choice of descriptors. The model also improves substantially on a previous study wherein a correlation ($R = 0.7$) was established between the acute toxicity (LD_{50}) and in vitro AChE potency of a group of direct-acting OP compounds (*29*), thus, demonstrating a

unique capacity of our model to handle those OP compounds that undergo biotransformation prior to interacting with AChE.

Contribution Analysis. To compare the relative importance of the terms included in eqs 1 and 2, we have relative importance values for each component (i.e., coefficients of the estimated normalized linear model) and have reported these quantities in Table 2. The CoMFA term is clearly the largest contribution to eq 2, with the next largest term, E(plg), having a relative weight of only 0.19. Given the fact that the CoMFA predictions, taken by themselves, correlate strongly ($R = 0.71$) with eq 1 (the phenomenological QSAR developed without a CoMFA contribution) it appears that much of this perceived dominance must actually result from functional overlap between features represented in the CoMFA model and those inherent in other descriptors. Adding a CoMFA term to the QSAR thus introduces some redundancy among descriptors and thereby reduces the proportional weights of any other descriptor that exhibits some degree of linear dependence with the CoMFA (in this case all of them). The large reduction in weight of the NASA term, for example, implies that it is so nearly completely described within the CoMFA as to contribute negligibly to the expression. This is not especially surprising, since CoMFA models frequently provide very good representations of three-dimensional electrostatic distributions. While we retain the NASA term within eq 2 for the sake of direct comparison to eq 1, we note that retraining the other descriptors in the absence of NASA yields an expression with values for R^2, Q^2, and coefficients for the other descriptors that are identical (within the significant figures reported herein) to those reported for eq 2. Furthermore, since descriptors based on molecular energy simultaneously represent multiple terms that may have varying levels of
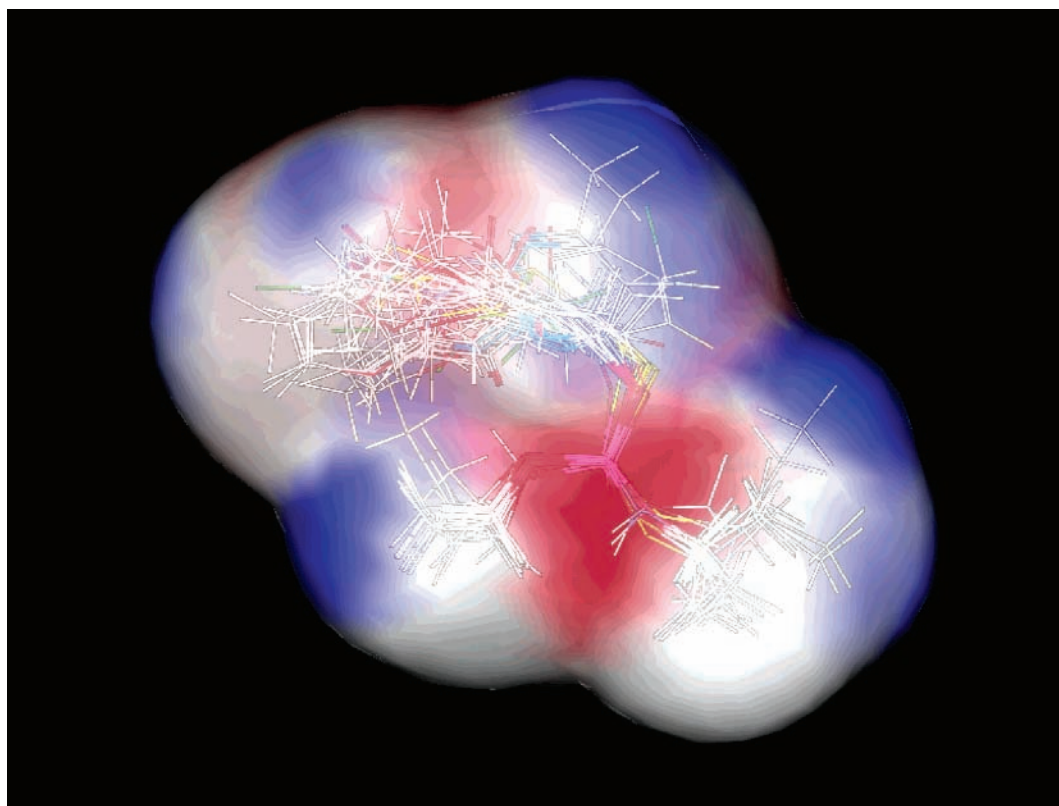
Figure 6. Interaction of molecular surface for OP compounds. Red regions indicate hydrophilic interactions, blue regions indicate exposed regions, and gray regions experience hydrophobic interactions.
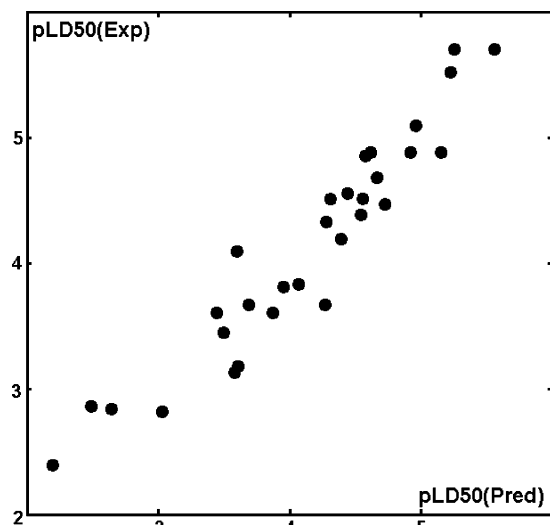

Figure 7. Correlation between the experimental and predicted pLD_{50} for the 30 OP compounds for the fully integrated model (eq 2).

Table 2. Relative Importance of the Descriptor in Eqs 1 and 2

| | relative weights | | |
terms	eq 1	eq 2	change
E(plg)	0.72	0.19	−74%
E(alg)	0.22	0.08	−64%
E(s203op)	0.38	0.08	−79%
E(met)	1.0	0.12	−88%
NASA	0.17	0.004	−98%
E(s203op_aged)	0.05	0.01	−80%
E(orig)	0.05	0.01	−80%
CoMFA	−	1.00	+100%

descriptor (its coefficient weight and possibly even sign) within a QSAR may change upon integration of CoMFA into the model. Because of such effects, eq 2, although a predictive tool of exceptional value, is less amenable to intuitive physical interpretation than the purely phenomenological eq 1. We will thus restrict our interpretive analysis to trends observed in eq 1.

In eq 1, E(met) and E(plg) are assigned the largest weights, while E(s203op_aged) and E(orig) appear to be the least important descriptors. This observation is consistent with the mechanism of actual OP toxicity. For E(plg) versus E(s203op_aged), the physical rationale for these weights is quite clear: structures of the aged complexes vary fairly little across the set of 30 toxins, whereas the phosphorylation leaving group contains much of the molecular diversity present in this collection. For E(met) versus E(orig), an important kinetic relationship is suggested: if the parent compound energies ultimately have relatively small contributions on the QSAR, it suggests that their respective metabolic reactions may all share a similar activation energy, whereas the importance of E(met) suggests that the reverse activation barrier may have substantially greater diversity. E(met) also must be considered as descriptor of relevance to the subsequent phosphorylation process (i.e., in this case modeling the reactant); thus in effect, it contributes twice to the equation.

Conclusions

Molecular modeling has been used herein to investigate the mechanism of acute toxicity of the OP compounds via the construction of a number of QSAR models to account for available LD_{50} data. A purely phenomenological QSAR model describing the toxic process as a function of ADME and covalent bonding processes was constructed as a seven-parameter model wherein ADME effects were modeled as the reactant and

correlative redundancy relative to the CoMFA (i.e., molecular electrostatic and van der Waals effects are also represented in CoMFA, but bond energy is not), the coefficient for that

product energies for the incumbent biotransformation reaction, plus the ligand negative accessible surface area, and the covalent phosphorylation and aging reactions were approximated by thermochemical characterization. This model achieved a correlation of $R^2 = 0.49$ relative to experiment, suggesting that the relationship is statistically valid but, lacking an account of the initial ligand−receptor Michaelis complex formation, likely not of great predictive value.

Given the unreliability of using docking methods to evaluate affinities for precovalent Michaelis complexes, we chose to account for this effect via a CoMFA pseudointeraction field. Without suitable in vitro affinity data covering our full training set, we chose to fit the CoMFA model directly to the LD_{50}, achieving a surprisingly strong correlation with experiment ($R^2 = 0.89$), thus, indicating that the pharmacophoric fit between receptor and ligand is a key factor in determining toxic inhibition of the AChE enzyme. However the CoMFA's marginal predictivity ($Q^2 = 0.57$) clearly reflects a need for a more rigorous account of ADME effects and subsequent covalent binding processes. With all parameters considered together (ADME, covalent, and CoMFA), both correlation ($R^2 = 0.90$) and predictivity ($Q^2 = 0.82$) are strong.

While the unified model is of substantial predictive value, it does come at the expense of interpretive ease: while spatial aspects of the CoMFA reproduce AChE inhibition phenomena that have been previously observed from structure-based analysis, correlative redundancy between the CoMFA and the various phenomenological descriptors tends to produce nonintuitive weights and signs that partially obscure the role of the various terms. For this reason, the purely phenomenological (non-CoMFA) model remains of some rhetorical value, providing some guidance as to the relative importance of different ADME and covalent binding effects.

The fact that both our phenomenological and composite models exhibit reasonable correlation with existing LD_{50} data despite approximating the efficacy of multiple enzymatic and covalent inhibition reactions via thermochemistry rather than kinetic activation barriers may suggest that the reactive processes must largely achieve equilibrium within the time frame under which the in vivo studies were carried out—a fact that puts more weight on the relative energetics of product and reaction than on the actual reaction barrier. This assessment deserves further analysis through explicit quantum chemical transition state calculations that are planned as a future study. Our fairly simplistic ADME model is another area for potential improvement. Indications are that our metabolic representation is reasonable; however, the blanket representation of other absorption, distribution, and excretion effects via single NASA is a major approximation. While the CoMFA appeared to be surprisingly adept at encoding such ADME trends, it is highly unlikely that it recovered all relevant effects. For example, one factor of significant possible interest to AChE inhibition research that may not have been adequately accounted for is blood−brain barrier (BBB) transmission. Identification of a convenient and apt BBB descriptor may further improve the model.

Rigorously addressing all potential model refinements may constitute a computationally unwieldy paradigm. While such refinement should nonetheless be pursued for the sake of a complete understanding of the OP toxicity mechanism, it is our short-term hope that the relative computational simplicity of this current model, as well as its reasonable predictive capacity, will permit rapid and reliable evaluation of other prospective toxins. The simpler phenomenological model also pinpoints trends in the relative importance of different factors on the acute toxicity but does make substantial approximations and leaves some details of the specific effects rather opaque. In the interests of full understanding of the acute toxicity, we are considering some additional factors, including the influence of water on the catalytic reaction within AChE, dynamic conformational changes in the active site, and transport kinetics governing how the OP compounds access the catalytic triad. In addition, mutagenesis work suggests that the peripheral anionic site may affect the rate constant by interacting with the cationic aging leaving group at Asp74 in human AChE (*30*). Finally, the details relating to the binding of the anionic phosphorylation leaving group may also prove to be of interest.

Supporting Information Available: All terms used in eqs 1 and 2 for each compound have been provided as Supporting Information. All structures for the toxins, metabolites, complexes, and leaving groups are available upon request. This material is available free of charge via the Internet at http://pubs.acs.org.

References

(1) Flanagan, J., and Jones, A. L. (2001) *Antidotes*, pp 87−114, Taylor and Francis, London and New York.

(2) Ehrich, M. (1998) Organophosphates. In *Encyclopedia of Toxicology* (Wexler, P., Ed.) pp 467−471, Academic Press, San Diego, CA.

(3) Sidell, F. R., and Borak, J. (1992) Chemical warfare agents: II. Nerve agents. *Ann. Emerg. Med. 21*, 865−871.

(4) Marrs, T. C. (1993) Organophosphate poisoning. *Pharmacol. Ther. 58*, 51−66.

(5) Sussman, J. L., Harel, M., Frolow, F., Oefner, C., Goldman, A., Toker, L., and Silman, I. (1991) Atomic structure of acetylcholinesterase from *Torpedo californica*: a prototypic acetylcholine-binding protein. *Science 253*, 872−879.

(6) Kovarik, Z., Radic, Z., Berman, H. A., Simeon-Rudolf, V., Reiner, E., and Taylor, P. (2003) Acetylcholinesterase active centre and gorge conformations analysed by combinatorial mutations and enantiomeric phosphonates. *Biochem. J. 373*, 33−40.

(7) Gilson, M. K., Straatsma, T. P., McCammon, J. A., Ripoll, D. R., Faerman, C. H., Axelsen, P. H., Silman, I., and Sussman, J. L. (1994) Open "back door" in a molecular dynamics simulation of acetylcholinesterase. *Science 263*, 1276−1278.

(8) Pope, C. N. (1999) Organophosphorus pesticides: do they all have the same mechanism of toxicity? *J. Toxicol. Environ. Health, Part B 2*, 161−181.

(9) Knaak, J. B., Dary, C. C., Power, F., Thompson, C. B., and Blancato, J. N. (2004) Physicochemical and biological data for the development of predictive organophosphorus pesticide QSARs and PBPK/PD models for human risk assessment. *Crit. Rev. Toxicol. 34*, 143−207.

(10) Barril, X., Orozco, M., and Luque, F. J. (2001) Towards improved acetylcholinesterase inhibitors: a structural and computational approach. *Mini Rev. Med. Chem. 1*, 255−266.

(11) Kua, J., Zhang, Y., and McCammon, J. A. (2002) Studying enzyme binding specificity in acetylcholinesterase using a combined molecular dynamics and multiple docking approach. *J. Am. Chem. Soc. 124*, 8260−8267.

(12) Guo, J.-X., Hurley, M. M., Wright, J. B., and Lushington, G. H. (2004) A docking score function for estimating ligand-protein interactions: application to acetylcholinesterase inhibition. *J. Med. Chem. 47*, 5492−5500.

(13) Berman, H. M., Westbrook, J., Feng, Z., Gilliland, G., Bhat, T. N., Weissig, H., Shindyalov, I. N., and Bourne, P. E. (2000) The protein data bank. *Nucleic Acids Res. 28*, 235−242.

(14) Millard, C. B., Koellner, G., Ordentlich, A., Shafferman, A., Silman, I., and Sussman, J. L. (1999) Reaction products of acetylcholinesterase and VX reveal a mobile histidine in the catalytic triad. *J. Am. Chem. Soc. 121*, 9883−9884.

(15) Bourne, Y., Taylor, P., Radic, Z., and Marchot, P. (2003) Structural insights into ligand interactions at the acetylcholinesterase peripheral anionic site. *EMBO J. 22*, 1−12.

(16) Legay, C., Bon, S., Vernier, P., Coussen, F., and Massoulie, J. (1993) Cloning and expression of a rat acetylcholinesterase subunit: generation of multiple molecular forms and complementarity with a Torpedo collagenic subunit. *J. Neurochem. 60*, 337−346.

(17) Weiner, S. J., Kollman, P. A., Nguyen, D. T., and Case, D. A. (1986) An all atom force field for simulations of proteins and nucleic acids. *J. Comput. Chem. 7*, 230−252.

(18) Halgren, T. A. (1999) MMFF VI. MMFF94s option for energy minimization studies. *J. Comput. Chem. 20*, 720−729.

(19) *Molecular Opperating Enviroment (MOE)*, version 2004.03, Chemical Computing Group, Inc., Montreal, Quebec, Canada, Mar, 2004.

(20) Dewar, M. J. S., Zoebisch, E. G., Healy, E. F., and Stewart, J. J. P. (1995) AM1: a new general purpose quantum mechanical model. *J. Am. Chem. Soc. 107*, 3902−3909.

(21) Stewart, J. J. P. (1993) *MOPAC7*, version 7, Stewart Computational Chemistry, Colorado Springs, CO.

(22) Ferguson, D. M., and Raber, D. J. (1989) A new approach to probing conformational space with molecular mechanics: random incremental pulase search. *J. Am. Chem. Soc. 111*, 4371−4378.

(23) *SIMCA-P*, Umereics AB, Umea, Sweden, July, 2001.

(24) Van der Waterbeemed, H., and Kansy, M. (1992) Hydrogen-bonding capacity and brain pentration. *Chimia 46*, 299−303.

(25) Hou, T. J., Zhang, W., Xia, K., Qiao, X. B., and Xu, X. J. (2004) ADME evaluation in drug discovery. 5. Correlation of Caco-2 permeation with simple molecular properties. *J. Chem. Inf. Comput. Sci. 44*, 1585−1600.

(26) Liu, R., Sun, H., and So, S.-S. (2001) Development of quantitative structure−property relationship models for early ADME evaluation in drug discovery. 2. Blood−brain barrier penetration. *J. Chem. Inf. Comput. Sci. 41*, 1623−1632.

(27) Barak, D., Ordentlich, A., Kaplan, D., Barak, R., Mizrahi, D., Kronman, C., Segall, Y., Velan, B., and Shafferman, A. (2000) Evidence for P−N bond scission in phosphoroamidate nerve agent adducts of human acetylcholinesterase. *Biochemistry 39*, 1156−1161.

(28) Ordentlich, A., Barak, D., Kronman, C., Benschop, H. P., De Jong, L. P., Ariel, N., Barak, R., Segall, Y., Velan, B., and Shafferman, A. (1999) Exploring the active center of human acetylcholinesterase with stereomers of an organophosphorus inhibitor with two chiral centers. *Biochemistry 38*, 3055−3066.

(29) Holmstedt, B. (1963) Structure−activity relationship of the organophosphorus anticholinesterase agents. *Handb. Exp. Toxicol. 15*, 428−485.

(30) Ordentlich, A., Barak, D., Sod-Moriah, G., Kaplan, D., Mizrahi, D., Segall, Y., Kronman, C., Karton, Y., Lazar, A., Marcus, D., Velan, B., and Shafferman, A. (2004) Stereoselectivity toward VX is determined by interactions with residues of the acyl pocket as well as of the peripheral anionic site of AChE. *Biochemistry 43*, 11255−11265.

(31) Yamanaka, S., Ohta, K., Tamita, Y., Takayanagi, A., Nomura, T., and Takaesu, Y. (1996) Effects on acute organophosphorus poisoning in rats in aging and solubility of organophosphates. *Environ. Health Prev. Med. 1*, 119−127.

(32) Lin, S. N., Chen, C. Y., Murphy, S. D., and Caprioli, R. M. (1980) Quantitative high-performance liquid chromatography and mass spectrometry for the analysis of the in vitro metabolism of the insecticide azinphos-methyl (guthion) by rat liver homogenates. *J. Agric. Food Chem. 28*, 85−88.

(33) Lucier, G. W., and Menzer, R. E. (1970) Nature of oxidative metabolites of dimethoate formed in rats, liver microsomes, and bean plants. *J. Agric. Food Chem. 18*, 698−704.

(34) Ivey, M. C., and Mann, H. D. (1975) Gas−liquid chromatographic determination of ethion, ethion monooxon, and ethion dioxon in tissues of turkeys and cattle. *J. Agric. Food Chem. 23*, 319−321.

(35) Krueger, H. R., and O'Brien, R. D. (1959) Relation between metabolism and differential toxicity of malathion in insects and mice. *J. Econ. Entomol. 52*, 1063−1067.

(36) Chopade, H. M., and Dauterman, W. C. (1981) Studies on the in vitro metabolism of methidathion by rat and mouse liver. *Pestic. Biochem. Physiol. 15*, 105−119.

(37) Venkatesh, K., Levi, P. E., Inman, A. O., Monteiro-Riveiere, N. A., Misra, R., and Hodgson, E. (1992) Enzymic and immunohistochemical studies on the role of cytochrome p450 and the flavin-containing monooxygenase of mouse skin in the metabolism of pesticides and other xenobiotics. *Pestic. Biochem. Physiol. 43*, 53−66.

(38) De Potas, G. M., and de D'Angelo, A. M. P. (1993) Phosphoinositide phosphorylation and shape changes produced by phosmet-oxon in human erythrocytes. *Comp. Biochem. Physiol., Part C: Pharmacol., Toxicol. Endocrinol. 106*, 561−566.

(39) Clark, D. E., Ivie, G. W., Crookshank, H. R., and Devaney, J. A. (1979) Effects of sulprofos and its sulfoxide and sulfone metabolites on laying hens fed the compounds in the diet. *J. Agric. Food Chem. 27*, 103−107.

(40) Li, J.-T., Sheng, S.-J., and Du, X.-L. (1999) Metabolism of terbufos in rat liver. *J. Occup. Health 41*, 62−68.

(41) Fukuto, T. R. (1978) Insecticide metabolism and mode of action. *Pure Appl. Chem. 50*, 9−10.

(42) Beike, J., Ortmann, C., Meiners, T., Brinkmann, B., and Kohler, H. (2002) LC_MS determination of oxydemeton-methyl and its main metabolite demeton-s-methylsulfon in biological sepcimens-applicatin to a forensic case. *J. Anal. Toxicol. 25*, 308−312.

(43) Gotoh, M., Sakata, M., Endo, T., Hayashi, H., Seno, H., and Suzuki, O. (2001) Profenofos metabolites in human poisoning. *Forensic Sci. Int. 116*, 221−226.

(44) Abu-Qare, A. W., and Abou-Donia, M. B. (2001) Quantification of nicotine, chlorpyrifos and their metabolites in rat plasma and urine using high-performance liquid chromatography. *J. Chromatogr., B: Biomed. Sci. Appl. 757*, 295−300.

(45) Osman, A. Z., Zayed, S. M. A. F. D., and Hazzaa, N. I. (1986) Fate and metabolism of the radiolabeled insecticide coumaphos in egyptian lactating goats. *Isot. Radiat. Res. 18*, 139−146.

(46) Kappers, W. A., Edwards, R. J., Murray, S., and Boobis, A. R. (2001) Diazinon is activated by CYP2C19 in human liver. *Toxicol. Appl. Pharmacol. 177*, 68−76.

(47) Sultatos, L. G. (1991) Metabolic activation of the organophosphorus insecticides chlorpyrifos and fenitrothion by perfused rat liver. *Toxicology 68*, 1−9.

(48) Cabras, P., Plumitallo, A., and Spanedda, L. (1991) High-performance liquid chromatographic separation of fenthion and its metabolites. *J. Chromatogr. 540*, 406−410.

(49) Bakke, J. E., and Price, C. E. (1976) Metabolism of O, O-dimethyl-O−(3,5,6-trichloro-2-pyridyl)phosphorothioate in sheep and rats and of 3,5,6-trichloro-2-pyridinol in sheep. *J. Environ. Sci. Health, Part B 11*, 9−22.

(50) Abu-Qare, A. W., and Abou-Donia, M. B. (2000) Urinary excretion of metabolites following a single dermal dose of [14C]methyl parathion in pregnant rats. *Toxicology 150*, 119−127.

(51) Soranno, T. M., and Sultatos, L. G. (1992) Biotransformation of the insecticide parathion by mouse brain. *Toxicol. Lett. 60*, 27−37.

(52) Berealey, C. J., and Lawrence, D. K. (1979) High-performance liquid chromatography of pirimiphos methyl and five metabolites. *J. Chromatogr. 168*, 461−469.

(53) Gorder, G. W., Kirino, O., Hirashima, A., and Casida, J. E. (1986) Bioactivation of isofenphos and analogs by oxidative N-dealkylation and desulfuration. *J. Agric. Food Chem. 34*, 941−947.